Cell Reports

Article

ABL allosteric inhibitors synergize with statins to enhance apoptosis of metastatic lung cancer cells

Graphical abstract

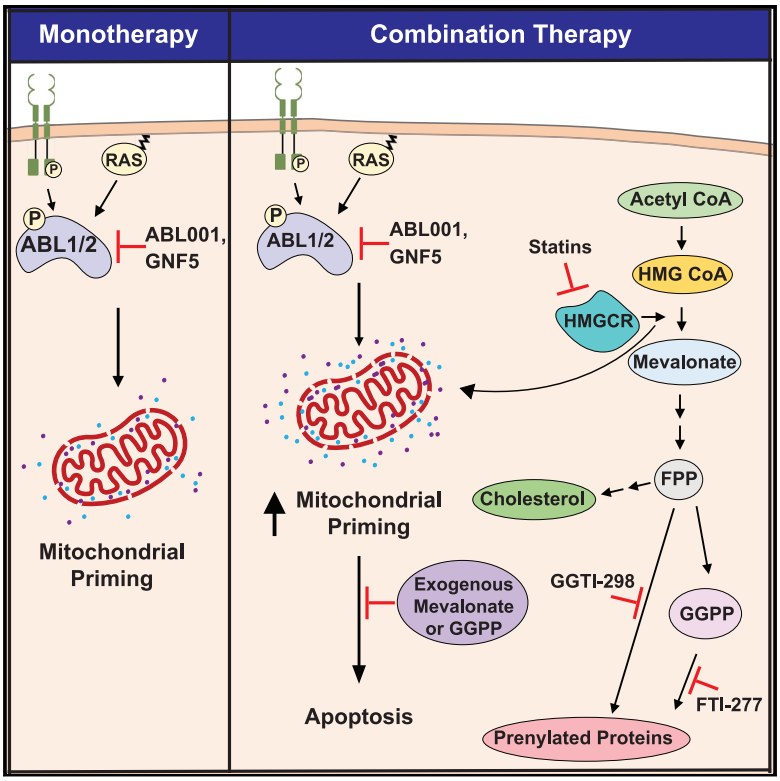

Authors

Jillian Hattaway Luttman, Jacob P. Hoj, Kevin H. Lin, ..., Nancie J. MacIver, Kris C. Wood, Ann Marie Pendergast

Correspondence

ann.pendergast@duke.edu

In brief

Metabolic reprogramming in tumors is an adaptation that generates vulnerabilities that can be exploited for developing new therapies. Here Luttman et al. identify synergism between ABL allosteric inhibitors and lipophilic statins to impair metastatic lung cancer cell outgrowth and colonization, leading to increased survival in mouse models of advanced disease.

Highlights

- ABL kinase allosteric inhibitors induce mitochondrial-mediated apoptosis
- HMG-CoA reductase inactivation synergizes with ABL allosteric inhibitors to induce apoptosis
- Isoprenoid pathway rescues cell survival upon cotreatment with statin and ABL001
- Cotreatment of ABL001 and simvastatin decreases metastases in mouse models

Luttman et al., 2021, Cell Reports *37*, 109880
October 26, 2021
https://doi.org/10.1016/j.celrep.2021.109880

CellPress

Cell Reports

CellPress
OPEN ACCESS

Article

ABL allosteric inhibitors synergize with statins to enhance apoptosis of metastatic lung cancer cells

Jillian Hattaway Luttman,[1] Jacob P. Hoj,[1] Kevin H. Lin,[1] Jiaxing Lin,[2] Jing Jin Gu,[1] Clay Rouse,[3] Amanda G. Nichols,[4] Nancie J. MacIver,[1,4,5] Kris C. Wood,[1,2] and Ann Marie Pendergast[1,2,6,*]

[1]Department of Pharmacology and Cancer Biology, Duke University School of Medicine, Durham, NC, USA
[2]Duke Cancer Institute, Duke University School of Medicine, Durham, NC, USA
[3]Division of Laboratory Animal Resources, Duke University School of Medicine, Durham, NC, USA
[4]Department of Pediatrics, Duke University School of Medicine, Durham, NC, USA
[5]Department of Immunology, Duke University School of Medicine, Durham, NC, USA
[6]Lead contact
*Correspondence: ann.pendergast@duke.edu
https://doi.org/10.1016/j.celrep.2021.109880

SUMMARY

Targeting mitochondrial metabolism has emerged as a treatment option for cancer patients. The ABL tyrosine kinases promote metastasis, and enhanced ABL signaling is associated with a poor prognosis in lung adenocarcinoma patients. Here we show that ABL kinase allosteric inhibitors impair mitochondrial integrity and decrease oxidative phosphorylation. To identify metabolic vulnerabilities that enhance this phenotype, we utilized a CRISPR/Cas9 loss-of-function screen and identified HMG-CoA reductase, the rate-limiting enzyme of the mevalonate pathway and target of statin therapies, as a top-scoring sensitizer to ABL inhibition. Combination treatment with ABL allosteric inhibitors and statins decreases metastatic lung cancer cell survival *in vitro* in a synergistic manner. Notably, combination therapy in mouse models of lung cancer brain metastasis and therapy resistance impairs metastatic colonization with a concomitant increase in animal survival. Thus, metabolic combination therapy might be effective to decrease metastatic outgrowth, leading to increased survival for lung cancer patients with advanced disease.

INTRODUCTION

Metabolic reprogramming is a hallmark of cancer and contributes to tumor development (Pavlova and Thompson, 2016). Oncogenic activation can increase the expression and activity of metabolic enzymes and transporters to meet the bioenergetic and biosynthetic needs of the cancer cell, thus creating metabolic vulnerabilities that might be exploited for emerging cancer therapies (DeBerardinis and Chandel, 2016; Dong et al., 2020; Jin et al., 2019; Pupo et al., 2019; Tarrado-Castellarnau et al., 2016). Among these dependencies is mitochondrial metabolism, which generates energy, regulates redox homeostasis, and provides key metabolites for macromolecule synthesis (Zong et al., 2016). While results from clinical trials evaluating the anticancer capability of drugs targeting mitochondrial metabolic pathways have shown potential benefits, the utility of these drugs is limited by the expression of transporters that facilitate import of these drugs into cancer cells, or toxicity associated with targeting mitochondrial metabolism not only in tumor cells but also in noncancerous tissue (Vasan et al., 2020).

Members of the Abelson (ABL) family of nonreceptor tyrosine kinases, ABL1 and ABL2, are activated downstream of diverse stimuli, including oncogenic drivers such as epidermal growth factor receptor (EGFR), human epidermal growth factor 2 (HER2), and kirsten rat sarcoma virus (KRAS), and promote progression and metastasis of solid tumor types, including lung and breast cancer (Gu et al., 2016, 2020; Hoj et al., 2019; Plattner et al., 1999: Khatri et al., 2019; Wang et al., 2016). ABL kinases promote cancer cell growth, survival, adhesion, and migration depending on the cellular context (Greuber et al., 2013; Wang and Pendergast, 2015). Recently, a role for ABL kinases in the regulation of mitochondria function was shown in HER2 amplified breast cancer cells, as HER2 promoted ABL-mediated tyrosine phosphorylation of mitochondrial creatine kinase 1 (MtCK1), leading to increased cellular energy production through the mitochondrial phosphocreatine shuttle (Kurmi et al., 2018). These findings suggested that inhibition of ABL signaling may uncover additional metabolic vulnerabilities in tumor cells.

Lung cancer is the leading cause of mortality among cancers worldwide in part due to the lack of actionable targets and transient responses to current therapies (Herbst et al., 2018). Here, we show that ABL kinases regulate mitochondrial function and integrity in lung adenocarcinoma cells harboring EGFR and KRAS mutations, and we also show that inactivation of ABL kinases impairs oxidative mitochondrial metabolism. As ABL inhibition impairs mitochondrial oxidation, we sought to

determine whether targeting metabolic pathways could enhance sensitivity to ABL allosteric inhibitors by performing a CRISPR/Cas9 loss-of-function screen targeting 2,322 metabolic enzymes and transporters. This screen identified 3-Hydroxy-3-methylglutaryl-coenzyme A reductase (HMGCR), a rate-limiting enzyme of the mevalonate (MVA) pathway and target of statin therapy, as a top-scoring sensitizer capable of potentiating cell death in the presence of sublethal doses of ABL allosteric inhibitors. Notably, we found that combination therapy of ABL kinase allosteric inhibitors with lipophilic statins impaired growth of clinically relevant therapy-resistant and brain-metastatic lung cancer cells in *in vitro* and *in vivo* mouse models. These results suggest new treatment avenues for lung cancer patients with advanced disease.

RESULTS

ABL kinase allosteric inhibitors regulate mitochondria function in lung cancer cells

We investigated whether inhibition of the ABL kinases could perturb mitochondrial function in lung adenocarcinoma cells with oncogenic mutations in EGFR, either sensitive to EGFR tyrosine kinase inhibitors (TKIs) (PC9) or TKI resistant (PC9 GR4), as well as KRAS mutant large cell lung carcinoma (LCC) H460 cells and KRAS mutant lung adenocarcinoma H358 cells. Lung cancer cells were analyzed for mitochondrial basal respiration, maximal respiration, and ATP production following treatment with ABL kinase inhibitors (Figures 1A–1D). For these studies, we used ABL allosteric inhibitors GNF5 and ABL001 (asciminib), which bind with high affinity to the unique myristate-binding pocket of the ABL kinases, as well as the second-generation ABL ATP-competitive inhibitor nilotinib (Deng et al., 2010; Zhang et al., 2010). Surprisingly, only the ABL allosteric inhibitors, but not nilotinib, markedly impaired mitochondria basal respiration, maximal respiration, and ATP production at all time points evaluated (Figures 1A–1D and S1A–S1E). The inability of nilotinib to inhibit mitochondria function might be due to the lack of specificity of ABL ATP-competitive inhibitors, as these drugs inhibit multiple enzymes other than ABL in solid tumors, and/or the inability of nilotinib to disrupt interactions with specific ABL downstream targets, which we showed can be blocked by ABL allosteric inhibitors through binding to a distinct site in the ABL kinase domain (Hoj et al., 2020). Moreover, treatment with ABL ATP-competitive inhibitors, but not allosteric inhibitors, induces activation of the RAF-ERK pathway in diverse cancer cell types (Gu et al., 2016; Packer et al., 2011; Wang et al., 2016). Notably, genetic knockdown of ABL1 and ABL2 (shAA) demonstrated that depletion of the ABL kinases similarly decreased mitochondrial respiration and ATP production in EGFR and KRAS mutant lung cancer cells (Figures 1E and S2A). Thus, depletion of ABL kinases phenocopied the ABL allosteric inhibitors by decreasing mitochondria function in lung cancer cells.

Next we evaluated whether aberrant mitochondria function induced by treatment with ABL allosteric inhibitors was also observed following treatment with two current US Food and Drug Administration (FDA)-approved therapeutics for lung adenocarcinoma patients: gefitinib, an EGFR TKI, and docetaxel, a taxane chemotherapy (Reck and Rabe, 2017). Lung cancer cells were treated with half-maximal inhibitory concentration (IC_{50}) drug doses to promote cell death as determined by dose-response assays (Table S1). Strikingly, mitochondrial function, as measured by basal and maximal respiration and ATP production, was greatly decreased following treatment with either GNF5 or ABL001 in lung cancer cells harboring EGFR or KRAS mutations (Figures 1A–1D) but was not impaired upon treatment with gefinitib or docetaxel in EGFR mutant PC9 parental cells and gefitinib-resistant PC9 GR4 cells (Figures 1A, 1B, S1D, and S1E). Additionally, treatment with docetaxel in KRAS mutant H460 and H358 lung cancer cells did not significantly impair mitochondria function (Figures 1C and 1D). Notably, while the ABL001 and GNF5 allosteric inhibitors markedly decreased mitochondrial function as measured by decreased mitochondrial respiration and impaired ATP production at all of the time points examined, treatment with gefitinib, nilotinib, and docetaxel failed to elicit these changes (Figures 1A–1D, S1D, and S1E). Next, we examined changes in basal and compensatory glycolysis in lung cancer cells following drug treatment. In contrast to nilotinib, gefitinib, and docetaxel which decreased basal and compensatory glycolysis in PC9 and PC9 GR4 cells, the ABL allosteric inhibitors did not inhibit glycolytic capacity in these cells (Figures S1F and S1G). Thus, ABL allosteric inhibitors impair mitochondria function.

To dissect the mechanism by which mitochondria function is impaired by ABL allosteric inhibitors, mitochondrial superoxide release was examined to identify changes in organelle integrity (Perillo et al., 2020; Zorov et al., 2014). We observed that mitochondrial reactive oxygen species (MitoROS) levels were increased upon GNF5 or ABL001 treatment, but not following gefitinib or docetaxel treatment, in EGFR mutant lung cancer cells sensitive or resistant to gefitinib therapy (Figures 1F and 1G). MitoROS levels were also increased in KRAS mutant H460 cells upon ABL allosteric inhibitor treatment, but not by docetaxel (Figure S2B). Thus, ABL allosteric inhibitors impair organelle integrity in lung cancer cells irrespective of the oncogenic driver (Figures 1F, 1G, and S2B). MitoROS levels were also increased following ABL1 and ABL2 knockdown in PC9 and H460 cells (Figures S2C and S2D). Analysis of mitochondria numbers following knockdown or pharmacologic inhibition of the ABL kinases did not show detectable changes in mitochondria numbers in PC9 and H460 cells, indicating that the decrease in the oxygen consumption rate (OCR) is not due to changes in mitochondrial density but rather mitochondria function (Figures S2E–S2H). Examination of changes in mitochondrial morphology by immunofluorescence staining with MitoTracker revealed that ABL001 caused a marginal, nonsignificant increase in mitochondrial network morphology, while the other drugs did not affect mitochondria length and width (Figures S2I and S2J).

Metabolically focused CRISPR/Cas9 loss-of-function screen identifies HMGCR inhibition with statin therapy as an apoptotic sensitizer to ABL allosteric inhibitors in lung cancer cells

Because inhibition of ABL kinases impairs oxidative mitochondrial metabolism, we sought to determine whether targeting additional metabolic nodes enhanced sensitivity to ABL

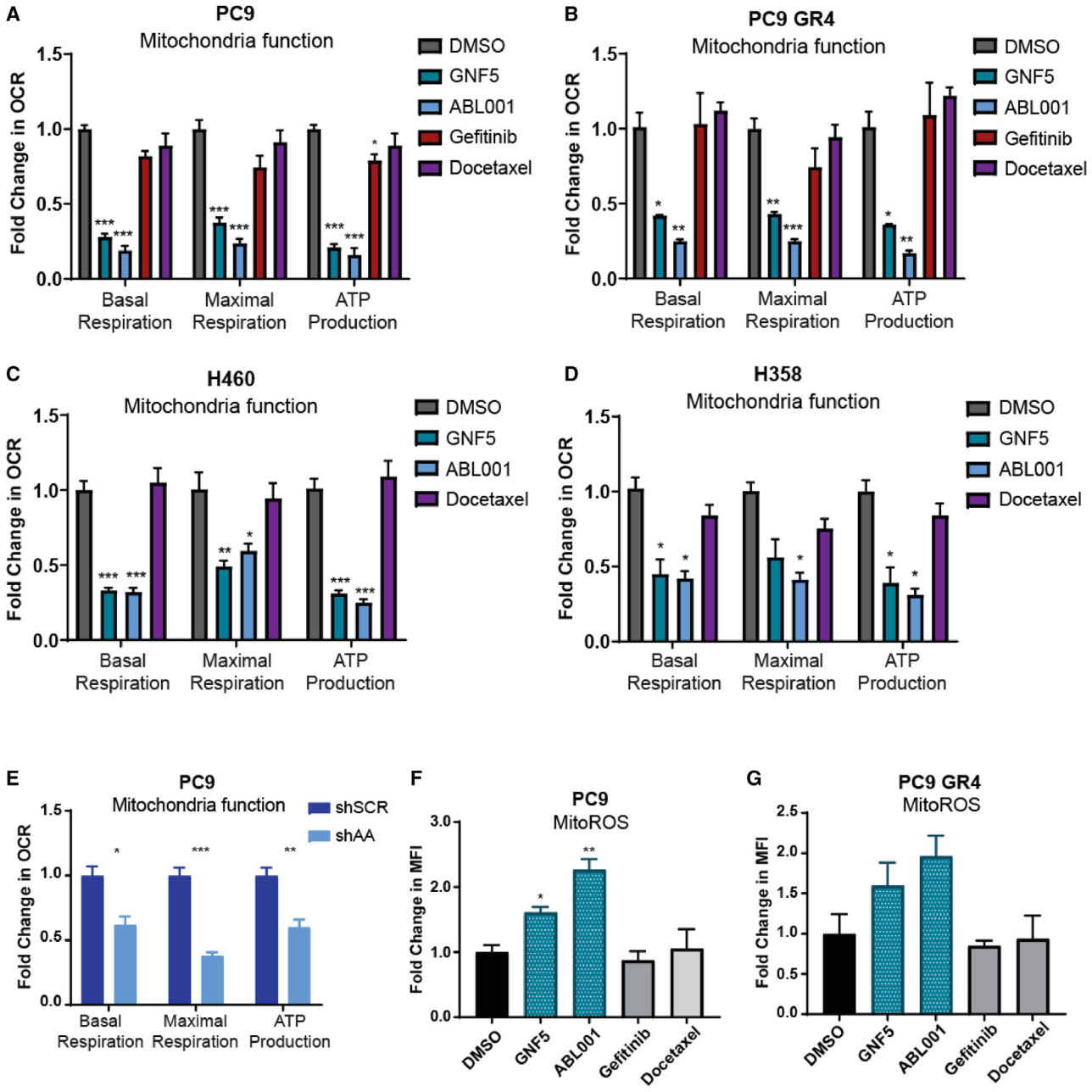

Figure 1. ABL kinase allosteric inhibitors regulate mitochondria function in lung cancer cells

(A–D) Seahorse XF Analyzer Mito Stress Test analysis of mitochondrial basal respiration, maximal respiration, and ATP production as measured by changes in oxygen consumption rate (OCR). Cells were treated with IC_{50} doses of each drug (see Table S1) for 24 h (n = 3). Data are the mean ± SEM.

(E) Mitochondrial basal respiration, maximal respiration, and ATP production as measured by Seahorse XF Analyzer's Mito Stress Test for PC9 cells harboring shRNAs against ABL1/ABL2 (shAA) and nontargeting control (shSCR) (n = 3). Data are the mean ± SEM.

(F and G) Mitochondrial ROS (MitoROS) release as measured by FACS analysis of median fluorescent intensity (MFI) using MitoSOX probe. Cells were treated with IC_{50} doses for 24 h (n = 3). Data are the mean ± SEM.

Statistical analysis was performed using one-way ANOVA and Tukey post hoc testing. *$p < 0.05$; **$p < 0.01$; ***$p < 0.001$. See also Figures S1, Figure S2, and Table S1.

inhibition. Thus, we employed a CRISPR/Cas9 loss-of-function screen targeting 2,322 metabolic enzymes and transporters (Lin et al., 2019) in the absence and presence of sublethal doses of the ABL allosteric inhibitor GNF5 that corresponded to a 20% loss in cell viability following a 3-day dose-response assay (Figure 2A). Library-transduced cells were puromycin selected and grown for 10 days prior to treatment. The cells were then exposed to either vehicle or GNF5 for 2 weeks, after which

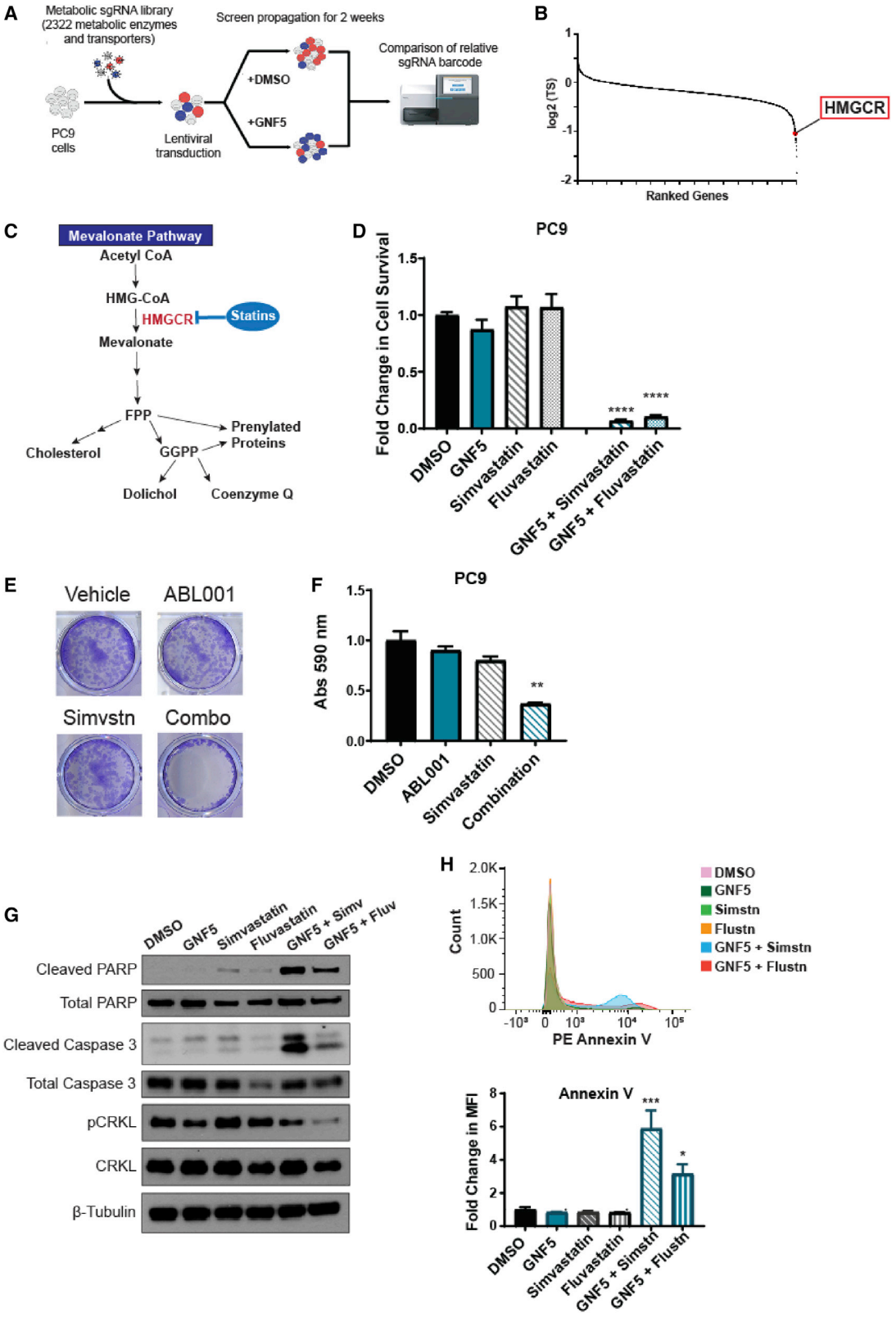

(legend on next page)

DNA was extracted from cell samples and polymerase chain reaction (PCR) was used to amplify and index barcode short guide RNA (sgRNA) amplicons, and the composition of sgRNA pools was deconvoluted through deep sequencing. The screen was validated for known essential genes by comparing the final and initial sgRNA pools in the vehicle-treated screen as previously described (Lin et al., 2019). Depletion metrics for each sgRNA were determined by normalizing the relative abundance of each construct following GNF5 treatment to the construct quantity present in vehicle-treated cells. The three most depleted constructs per gene were averaged to produce a gene-level three score (TS) as previously detailed (Lin et al., 2019) (Table S2). TS scores were ranked, allowing for identification of genes that were specifically depleted or enriched in the GNF5-treated cell population (Figure 2B). We focused on the subset of depleted genes that fell below the inflection point of the curve to experimentally evaluate whether loss of the top 5% of deleted genes could potentiate the cell-killing effects of ABL allosteric inhibition (Table S2). Among these hits were complexes of the electron transport chain as well as metabolic enzymes and transporters that converged on metabolic nodes that regulate cholesterol synthesis and mobilization. We focused on targets that could be pharmacologically inhibited with FDA-approved drugs, and we identified HMGCR, the rate-limiting enzyme of the MVA pathway, as a top-scoring reactive sensitizer to cell death in the presence of low-dose GNF5 (Figures 2B and 2C). We selected *HMGCR* for further study because it was in the top 1% of depleted genes and is the target of statin therapies commonly prescribed for patients with high cholesterol (Karr, 2017). Statins have a highly tolerable pharmacokinetic profile and availability, making HMGCR an attractive target for combination therapy.

To validate the results of the screen, PC9 cells were treated with sublethal doses of GNF5 and two statins, simvastatin and fluvastatin. Following 72 h of combination treatment, over 90% of cells underwent cell death (Figure 2D). Similar results were seen when cells were cultured in colony formation assays (Figures 2E, 2F, S3A, and S3B). To validate the on-target effect of statins, shRNAs against HMGCR were transduced into PC9 lung cancer cells, and these cells were then treated with GNF5 (Figures S3C and S3D). HMGCR was partially knocked down, allowing for the cells to remain viable albeit with reduced pathway activity. HMGCR knockdown exhibited markedly decreased cell survival compared to control lung cancer cells following treatment with GNF5 (Figures S3C and S3D), in agreement with the pharmacologic data. Further, immunoblotting revealed dramatic induction of the apoptotic mediators cleaved poly (ADP-ribose) polymerase (PARP) and cleaved caspase-3 following 24 h of combination treatment with GNF5 and statins, which was consistent with identification of apoptotic cells by flow cytometry of Annexin V-stained lung cancer cells cotreated with GNF5 and statins (Figures 2G and 2H). These data reveal a treatment paradigm whereby HMGCR inhibition combined with ABL allosteric inhibition sensitizes cells toward apoptotic cell death.

ABL allosteric inhibitors preferentially synergize with statins to induce lung cancer cell death

To assess whether ABL allosteric inhibitors might preferentially synergize with statins in comparison to EGFR inhibitors and chemotherapeutic drugs, lung cancer cells were treated at equivalent sublethal doses below the IC_{50} value of each drug as determined with dose-response assays for each cell line. Notably, only the ABL allosteric inhibitors exhibited enhanced cell-killing effects upon combination with either simvastatin or fluvastatin in EGFR mutant cells sensitive to EGFR TKIs (PC9), resistant to gefitinib (PC9 GR4), or harboring metastatic tropism to the brain (PC9 BrM3) (Figures 3A–3C). Similar findings were observed in KRAS mutant H460 and H358 cancer cell lines (Figures 3D and 3E). The combination of ABL allosteric inhibitors with statins was found to be synergistic across cell lines as assessed by the Bliss formula for synergy (Demidenko and Miller, 2019), where a score of 1 indicates true synergy (Figure 3F).

Next, we sought to evaluate whether sensitization to statin treatment was specific to the ABL allosteric inhibitors or could also be induced by ABL ATP-site inhibitors. Cotreatment of PC9 GR4 and H460 cells with sublethal doses of nilotinib and either simvastatin or fluvastatin did not promote additive or synergistic decreases in cell viability (Figures S3E and S3F). These findings highlight the differential effects induced by ABL allosteric versus ATP-competitive inhibitors, and they support the notion that ABL allosteric inhibitors preferentially sensitize lung

Figure 2. Metabolically focused CRISPR/Cas9 loss-of-function screen identifies inhibition of HMGCR with statin therapy as an apoptotic sensitizer in the presence of ABL allosteric inhibitors

(A) Diagram of CRISPR/Cas9 loss-of-function screening strategy adapted from (Lin et al., 2019).

(B) Gene-level representation of GNF5 sensitization phenotype. Genes were ranked by their log2-transformed three score (TS) (GNF5-treated/DMSO-treated). Apoptotically reactive genes are denoted in red and HMGCR TS is highlighted.

(C) Schematic of the mevalonate pathway indicating statin inhibition of HMGCR.

(D) Pharmacologic sensitization of statin therapeutics to GNF5-mediated cell death using 72-h growth inhibition assays. Shown are sublethal doses of GNF5 (5 μM), simvastatin (1 μM), and fluvastatin (0.5 μM) derived from 72-h dose-response curves in the presence and absence of each drug (n = 3). Data are the mean ± SEM.

(E) Representative images from colony formation assays of PC9 cells treated with ABL001 (1 μM) and simvastatin (100 nM) alone and in combination for 1 week (n = 2).

(F) Quantification of absorbance readings for colony formation assays from E (n = 2). Data are the mean ± SEM.

(G) Immunoblots of cleaved PARP, cleaved caspase-3, and β-tubulin in PC9 cells treated for 24 h with GNF5 (5 μM), simvastatin (1 μM), and fluvastatin (0.5 μM) alone and in combination (n = 3).

(H) FACS of total events and relative change in Annexin V+ PC9 cells treated for 24 h with GNF5 (5 μM), simvastatin (1 μM), and fluvastatin (0.5 μM) alone and in combination. The graph (bottom) shows the fold change in Annexin V staining (n = 3). Data are the mean ± SEM.

Statistical analysis was performed using one-way ANOVA and Tukey post hoc testing. *$p < 0.05$; **$p < 0.01$; ***$p < 0.001$; ****$p < 0.0001$. See also Figure S3.

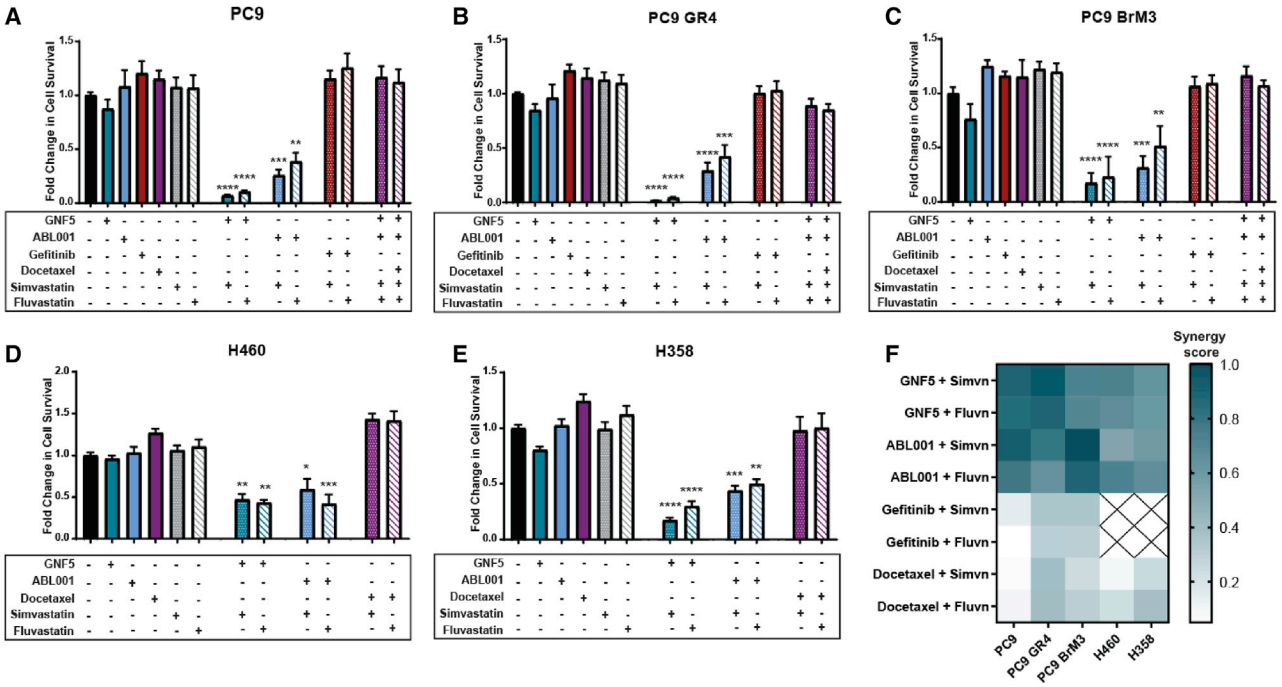

Figure 3. ABL allosteric inhibitors preferentially synergize with statins to induce lung cancer cell death

(A–E) Comparison of pharmacologic sensitization of statin therapeutics to ABL allosteric inhibitors versus FDA-approved therapies using 72-h growth inhibition assays. Shown are sublethal doses of GNF5 (5 μM for PC9, PC9 GR4, and PC9 BrM3; 7.5 μM for H460 and H358), ABL001 (5 μM for PC9, PC9 GR4, and PC9 BrM3; 7.5 μM for H460 and H358), gefitinib (7.5 nM for PC9 and PC9 BrM3; 100 nM for PC9 GR4), docetaxel (0.5 nM for PC9, PC9 GR4, PC9 BrM3, and H358; 0.25 nM for H460), simvastatin (1 μM for PC9, PC9 GR4, and PC9 BrM3; 3 μM for H460 and H358), and fluvastatin (0.5 μM for PC9, PC9 GR4, and PC9 BrM3; 2 μM for H460 and H358), derived from 72-h dose-response curves in the presence and absence of each drug (n = 3). Data are the mean ± SEM. Statistical analysis was performed using one-way ANOVA and Tukey post hoc testing. *p < 0.05; **p < 0.01; ***p < 0.001; ****p < 0.0001.

(F) Heatmap representing the synergy score for each drug interaction as calculated by the Bliss formula for synergy. A score of 1.0 indicates true synergy. See also Figure S4.

cancer cells to cell death *in vitro* by combination treatment with lipophilic statins.

There are conflicting *in vitro* reports indicating additive cell-killing effects of chemotherapy with high-dose statin therapeutics (Chou et al., 2019; Otahal et al., 2020). Thus, we treated lung cancer cells with IC_{50} doses of GNF5, ABL001, gefitinib, and docetaxel to determine whether treatment at higher than sublethal doses could enhance the cell-killing effects of these drugs. Again, we found that only ABL allosteric inhibitors could synergize with simvastatin and promote cleavage of PARP and caspase-3 in PC9 cells (Figures S4A–S4C). In this regard, clinical trial data have shown that statins in combination with various chemotherapies had either marginal or no effect on progression-free survival or overall survival in lung cancer patients (Han et al., 2011; Lee et al., 2017; Seckl et al., 2017). Together, these results show that in contrast to gefitinib and docetaxel, ABL allosteric inhibitors preferentially sensitize lung cancer cells to statins and dramatically inhibit cancer cell survival.

MVA, but not cholesterol, rescues cell survival in lung cancer cells cotreated with statins and ABL allosteric inhibitors

The MVA pathway catalyzes the conversion of acetyl-CoA to HMG-CoA, which is then converted by HMGCR into MVA (Figure 2C). MVA is required for the generation of cholesterol and isoprenoids among other end products. Rescue experiments were performed to identify whether MVA or the downstream metabolite cholesterol could reverse the cell-killing effect induced by low-dose simvastatin treatment in cells cotreated with sublethal doses of ABL allosteric inhibitors. Interestingly, only MVA, but not cholesterol, could rescue cell survival in PC9 GR4 and H460 lung cancer cells (Figures 4A and 4C). Consistent with these findings, the addition of MVA, but not cholesterol, prevented cleavage of PARP and caspase-3, suggesting that the sensitization of lung cancer cells to apoptosis induced by ABL allosteric inhibitors in combination with statin therapy is independent of cholesterol (Figures 4B and 4D).

The apoptotic cascade is mediated by interplay among BCL-2 family proteins composed of proapoptotic and antiapoptotic proteins (Warren et al., 2019). Following combination treatment with ABL allosteric inhibitors and statins, we observed that gene expression of the prosurvival factors BCL-2 and BCL-X_L was downregulated, while expression of proapoptotic p53 upregulated modulator of apoptosis (PUMA) was increased (Figure 4E). Supplementation with MVA, but not cholesterol, restored gene expression back to baseline (Figure 4E). Changes in BCL-2 family member expression can elicit pore formation in the mitochondria, resulting in mitochondria outer membrane permeabilization

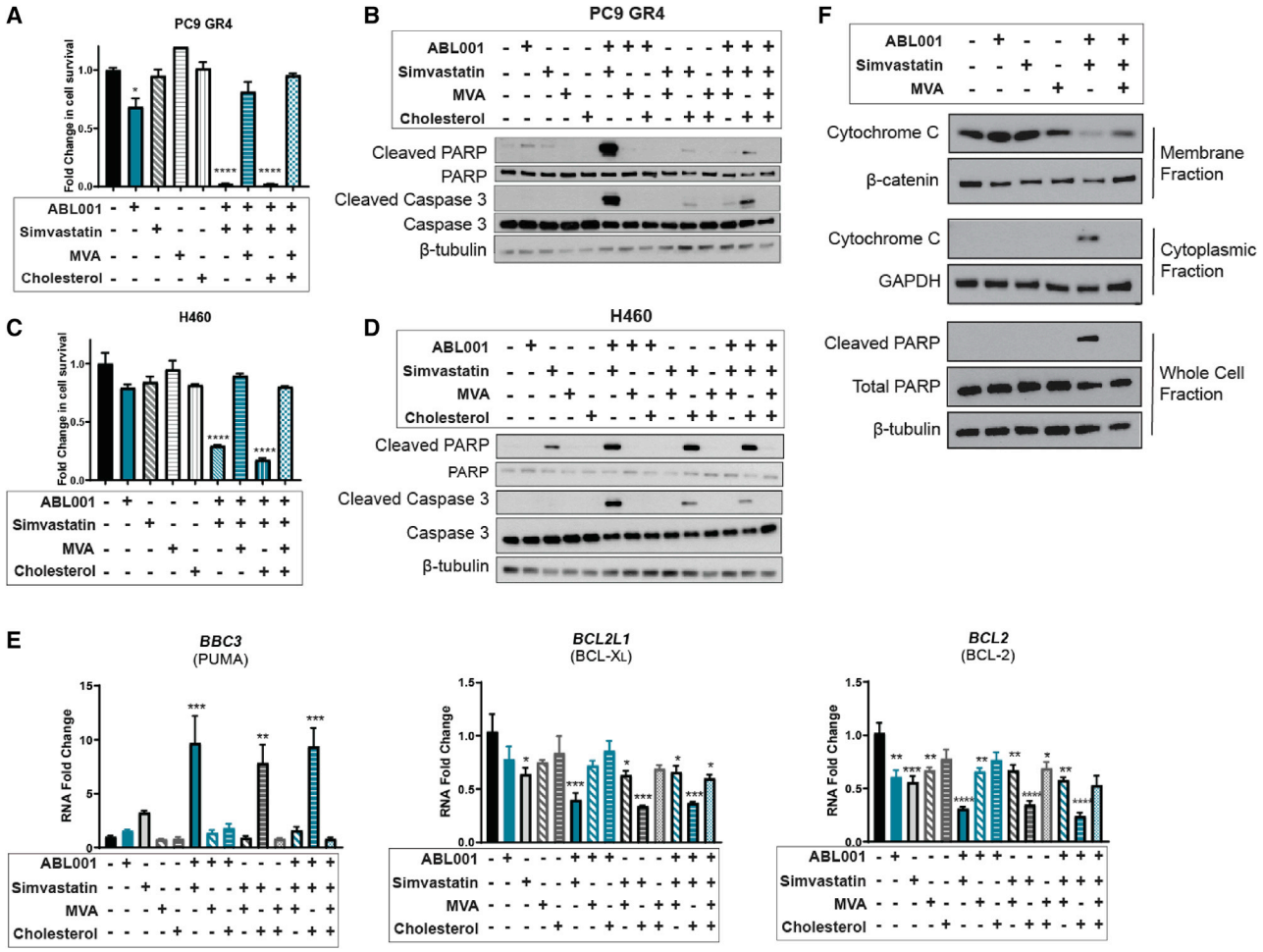

Figure 4. Mevalonate, but not cholesterol, rescues cell survival in lung cancer cells cotreated with statins and ABL allosteric inhibitors

(A) Cell viability of PC9 GR4 cells treated with the combination of 5 μM ABL001 and 1 μM simvastatin supplemented with 500 μM mevalonate (MVA) or 25 μM cholesterol for 72 h (n = 3). Data are the mean ± SEM.

(B) Immunoblots of cleaved PARP, cleaved caspase 3, and β-tubulin in PC9 cells treated for 24 h with 5 μM ABL001 and 1 μM simvastatin supplemented with 500 μM MVA or 25 μM cholesterol (n = 3).

(C) Cell viability of H460 cells treated with the combination of 7.5 μM ABL001 and 3 μM simvastatin supplemented with 500 μM MVA or 25 μM cholesterol for 72 h (n = 3).

(D) Immunoblots of cleaved PARP, cleaved caspase 3, and β-tubulin in H460 cells treated for 24 h with 7.5 μM ABL001 and 3 μM simvastatin supplemented with 500 μM MVA or 25 μM cholesterol (n = 3).

(E) qRT-PCR of indicated mRNAs in PC9 GR4 cells treated with 5 μM ABL001 and 1 μM simvastatin supplemented with 500 μM MVA or 25 μM cholesterol for 24 h. Statistical analysis was performed using one-way ANOVA and Fisher post hoc testing (n = 3). Data are the mean ± SEM.

(F) Immunoblots of cytochrome *c*, cleaved PARP, β-catenin, GAPDH, and β-tubulin. PC9 GR4 cells were treated with of 5 μM ABL001 and 1 μM simvastatin supplemented with 500 μM MVA for 24 h, collected, and fractionated. Cytoplasmic, membrane, and whole cell fractions are shown for drug treatments (n = 3). Statistical analysis was performed using one-way ANOVA and Tukey post hoc testing. *p < 0.05; **p < 0.01; ***p < 0.001; ****p < 0.0001.

(MOMP), leading to cytochrome *c* release (Garrido et al., 2006). Subcellular fractionation revealed release of cytochrome *c* from the mitochondrial membrane fraction into the cytosol in response to cotreatment with ABL001 and simvastatin, which was reversed following the addition of MVA (Figure 4F). These data show that ABL001 and simvastatin combination therapy alters gene expression of BCL-2 family members, leading to permeabilization of the mitochondria, release of cytochrome *c* into the cytosol, and cleavage of caspase 3, and that these processes can be reversed by the addition of MVA.

Apoptotic sensitization to statin therapy by ABL allosteric inhibitors requires inhibition of protein prenylation

MVA is the precursor to farnesyl diphosphate (FPP), which can either be converted to geranylgeranyl diphosphate (GGPP) or cyclized to produce squalene for cholesterol production (Thurnher et al., 2012). Both FPP and GGPP are metabolites in the isoprenoid pathway required for protein prenylation, a posttranslational enzymatic modification that adds a prenylated motif to CAAX proteins such as the RAP1A GTPase (Konstantinopoulos and

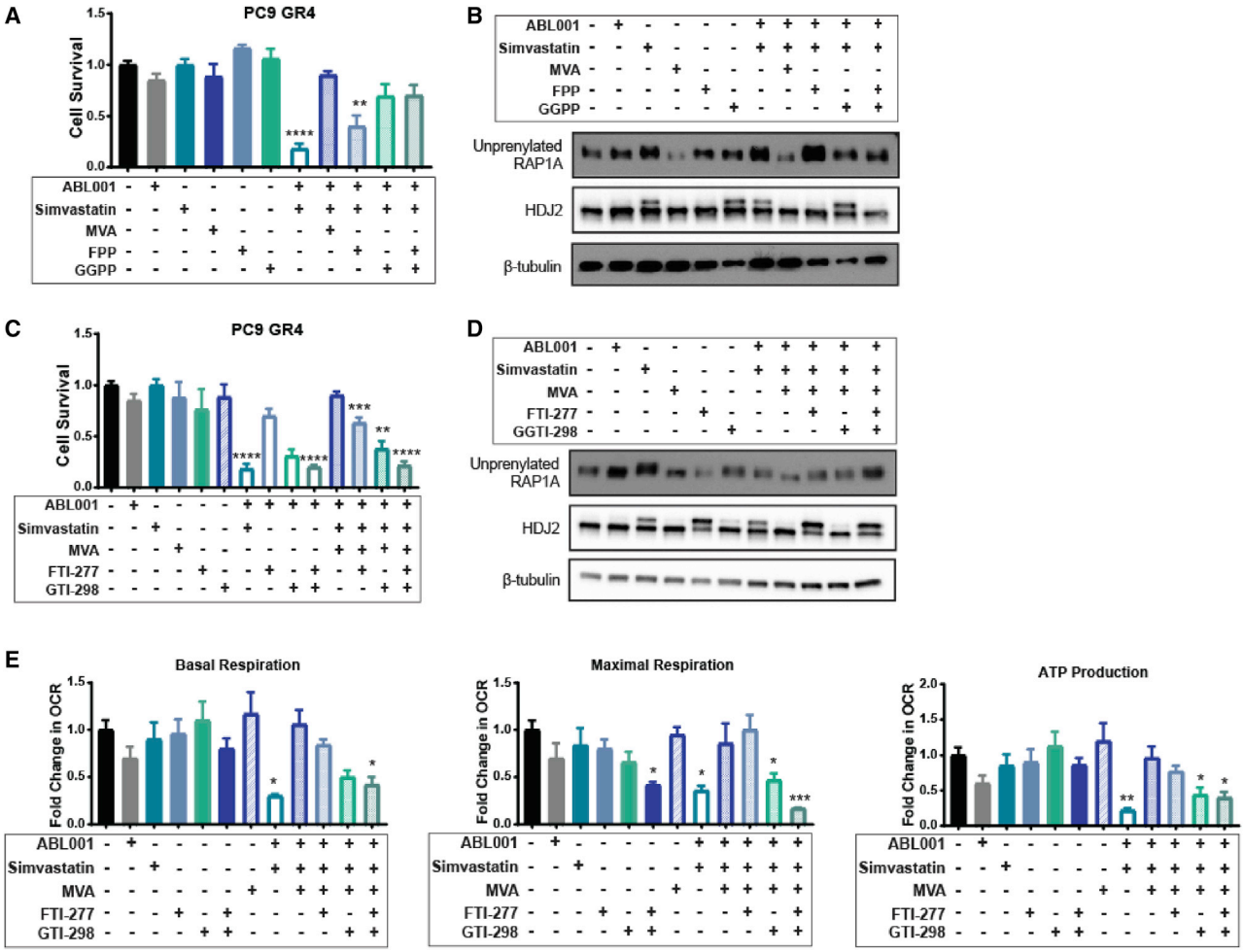

Figure 5. Apoptotic sensitization to statin therapy by ABL allosteric inhibitors requires inhibition of protein prenylation

(A) Cell viability of PC9 GR4 cells treated singly or with the combination of 5 μM ABL001 and 1 μM simvastatin supplemented with 500 μM MVA, 10 μM FPP, or 10 μM GGPP for 72 h (n = 3). Data are the mean ± SEM.

(B) Immunoblots of unprenylated RAP1A, HDJ-2, and β-tubulin in PC9 GR4 cells treated for 24 h with 5 μM ABL001 and 1 μM simvastatin supplemented with 500 μM MVA, 10 μM FPP (farnesylation metabolite), or 10 μM GGPP (geranylgeranylation metabolite). Simvastatin caused a mobility shift of HDJ-2 (slower, migrating unprenylated form) and induced the appearance of unprenylated RAP1A. Prenylation alterations were rescued with the indicated metabolites for each pathway (n = 3).

(C) Cell viability of PC9 GR4 cells treated with 5 μM ABL001 and 1 μM simvastatin, 500 μM MVA, 5 μM GGTI-298 (GGT inhibitor), and 12.5 μM FTI-277 (FT inhibitor) for 72 h (n = 3). Data are the mean ± SEM.

(D) Immunoblots of unprenylated RAP1A, HDJ-2, and β-tubulin in PC9 GR4 cells treated for 24 h with 5 μM ABL001 and 1 μM simvastatin supplemented with 500 μM MVA, 5 μM GGTI-298, and 12.5 μM FTI-277 (n = 3).

(E) Mitochondrial basal respiration, maximal respiration, and ATP production as measured by Seahorse XF Analyzer's Mito Stress Test for PC9 GR4 cells treated singly or with indicated combinations of 2.5 μM ABL001, 1 μM simvastatin, 500 μM MVA, 5 μM GGTI-298 (GGT inhibitor), or 12.5 μM FTI-277 for 24 h (n = 2). Data are the mean ± SEM.

Statistical analysis was performed using one-way ANOVA and Tukey post hoc testing. *p < 0.05; **p < 0.01; ***p < 0.001; ****p < 0.0001. See also Figure S5.

Papavassiliou, 2007). These modifications regulate protein localization to different cellular compartments, facilitate specific protein-protein interactions, and modulate protein stability. Since the downstream sterol metabolite cholesterol did not rescue cell survival, we investigated whether metabolites in the isoprenoid pathway were critical for sensitization to statin therapeutics. We found that the addition of GGPP preferentially rescued cell viability compared to FPP in PC9 GR4, PC9, and H460 cells co-treated with ABL001 and simvastatin (Figures 5A, S5A, and S5B).

Immunoblotting was performed to assess whether protein prenylation was altered following simvastatin treatment (Figure 5B). Simvastatin treatment increased levels of unprenylated RAP1A protein indicating inhibition of the geranylgeranylation pathway and induced a mobility shift in HDJ2 signifying inhibition of the farnesylation pathway, both of which were reversed by the addition of the indicated prenylation metabolites (Figure 5B) (Lobell et al., 2002; Munoz et al., 2017). We next tested whether inhibition of either geranylgeranyl transferase (GGT) or farnesyl

transferase (FT) could impact cell survival in a manner similar to simvastatin treatment. Survival of PC9 GR4, PC9, and H460 cells cotreated with ABL001 and a GGT-1 inhibitor (GGTI-298) was significantly impaired, but cell survival was only slightly decreased following the addition of the FT inhibitor (FTI-277) in the presence of ABL001 (Figures 5C, S5C, and S5D). Further, the nonadditivity observed for statin treatment and GGT and FT inhibition suggested that the synergizing effects of statins or GGTI-298 + FTI-277 in the presence of an ABL allosteric inhibitor operate through the same pathway. Immunoblotting confirmed that each inhibitor specifically suppressed its target pathway (Figure 5D). Collectively, these data reveal that inhibition of protein geranylgeranylation is sufficient to sensitize cells to ABL allosteric inhibitors, leading to enhanced intrinsic apoptosis.

Since we observed that oxidative metabolism was impaired following treatment with IC_{50} doses of the ABL allosteric inhibitors (Figure 1) and that combination therapy induced MOMP (Figure 4), we next investigated whether combination treatment with an ABL allosteric inhibitor and a statin affected mitochondrial metabolism and whether these effects might be due to changes in the protein prenylation pathway. To this end, we examined changes in mitochondrial respiration in cells cotreated with low doses of ABL001 and simvastatin and found that basal and maximal respiration as well as ATP production were decreased (Figure 5E). Notably, the addition of MVA restored mitochondrial respiration back to baseline; while treatment with FTI-277 had minimal effect, treatment with GGTI-298 negated the MVA rescue and caused mitochondrial respiration levels to decrease to a similar degree as to those observed following ABL001 and simvastatin treatment (Figure 5E). These data suggest that inhibition of the MVA pathway in combination with ABL kinase inhibition promotes cell death by impairing mitochondrial function.

Combination therapy of ABL001 and simvastatin impairs metastatic tumor growth and increases animal survival in mouse models of lung cancer brain metastasis and gefitinib resistance

Despite recent clinical successes with next-generation EGFR TKIs such as osimertinib, relapses often occur among patients harboring EGFR mutant non-small cell lung cancer cell (NSCLC). Moreover, patients harboring KRAS driver mutations have few tractable therapeutic options available (Kelly et al., 2018; Yang et al., 2019). Further, the ability of anticancer drugs to efficiently penetrate the blood-brain barrier (BBB) and reach therapeutic doses for lung cancer patients harboring brain metastases is limited. Thus, we chose to evaluate whether statins could synergize with ABL inhibitors *in vivo* to treat cancer cells seeded at distal sites following intracardiac injection in clinically relevant mouse models of brain metastasis and therapy resistance. We employed ABL001 as it has been shown to cross the BBB in preclinical mouse models and is currently in clinical trials for therapy-resistant patients with BCR-ABL+ chronic myeloid leukemia (Hoj et al., 2019; Hughes et al., 2019). Importantly, administration of ABL001 by oral gavage is well tolerated and does not induce weight loss in mice (Zhang et al., 2010). Pharmacokinetic data have shown that lipophilic statins can cross the BBB more readily than hydrophilic statins (Wood et al., 2010). In this regard, studies testing the ability of radiolabeled simvastatin to cross the BBB identified simvastatin-derived radioactivity in the rat brain following oral administration (Merck, 2020). Thus, we employed clinically relevant low doses of simvastatin and treated mice with 10 mg/kg simvastatin once a day, which is equivalent to doses used in humans (Barter, 2018; Björkhem-Bergman et al., 2011; Hu et al., 2012)

To determine whether combination treatment could impair brain-metastatic outgrowth, we used brain-metastatic PC9-BrM3 cells derived through serial rounds of intracardiac injection in athymic nude mice (Hoj et al., 2019). Previous studies have shown that following injection into the arterial circulation, brain-metastatic lung cancer cells extravasate into the brain parenchyma by day 6 postinjection (Kienast et al., 2010; Valiente et al., 2018). Thus, we performed bioluminescent imaging (BLI) on day 6 postintracardiac injection to stratify mice into treatment groups and began drug treatments on day 7 (Figure 6A). Mice were divided into four treatment groups: vehicle, ABL001, simvastatin, or a combination of ABL001 and simvastatin. We found that overall survival was significantly increased in mice harboring PC9-BrM3 brain metastases following combination treatment in comparison to vehicle, ABL001, or simvastatin alone (Figure 6B). Similar results were observed in mice harboring gefitinib-resistant PC9 cells (PC9 GR4), as ABL001 and simvastatin combination therapy extended overall survival (Figure 6C). Quantification of brain flux at day 27 revealed decreased disease burden in mice treated with both ABL001 and simvastatin compared to the vehicle or single drug treatment groups (Figures 6D and 6E). Immunofluorescence analysis of brain metastases for proliferation and apoptotic markers revealed decreased expression of the proliferative marker Ki67 and significantly increased expression of the cell death marker cleaved caspase-3 (Figures 6F–6H). Notably, the effect of combination drug treatment on subcutaneous xenograft tumor growth was minimal in comparison to the vehicle or single treatment groups for PC9 GR4 cells injected subcutaneously into the flank (Figures S6A and S6B). Quantification of vehicle- and drug-treated mice harboring orthotopic lung tumors following intrathoracic injections showed that the combination of ABL001 and simvastatin elicited a decrease in tumor burden, but this did not reach statistical significance (Figures S6C–S6E). These findings are consistent with previous reports showing that the inhibitory effects of ABL inactivation on primary tumor growth are cell context dependent and that genetic and pharmacologic inhibition of the ABL kinases predominantly decreased spontaneous metastasis (Gil-Henn et al., 2013; Meirson et al., 2018). Together, these data reveal that combination treatment with both ABL001 and simvastatin impairs metastatic outgrowth of lung cancer cells by enhancing tumor cell death.

DISCUSSION

Metabolic reprogramming in tumors is an adaptation that allows cancer cells to meet enhanced bioenergetic needs, but metabolic dysregulation also generates vulnerabilities in cancer cells that can be exploited for the development of treatment strategies. Among these vulnerabilities is mitochondrial oxidative metabolism, as cancer cells are reliant on functional

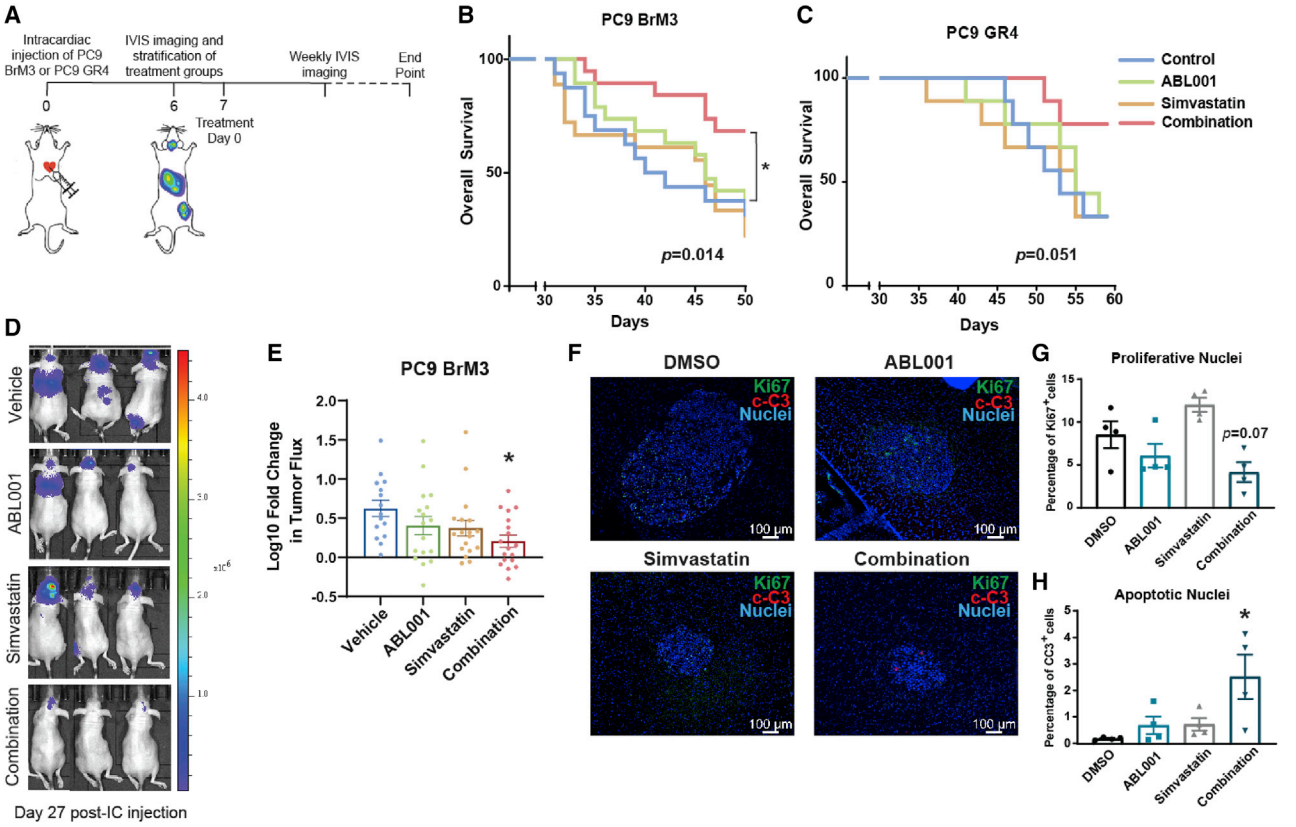

Figure 6. Combination therapy of ABL001 and simvastatin promotes tumor cell apoptosis and increases survival in mouse models of lung cancer brain metastasis and gefitinib resistance

(A) Schematic showing experimental overview. PC9 BrM3 or PC9 GR4 cells labeled with luciferase-tomato (pFULT) were intracardially injected into mice on day 0. IVIS imaging of metastatic burden was performed on day 6, followed by equivalent stratification of mice into treatment groups based on tumor flux. Oral gavage treatment of drugs began on day 7, followed by weekly IVIS imaging until the experimental end point. Statistical analysis of overall survival was calculated using log-rank (Mantel-Cox) test and interactions below an adjusted $p < 0.017$ were deemed significant, accounting for three pairwise comparisons.

(B) Overall survival of mice injected intracardially with PC9 BrM3-pFULT cells treated with DMSO (n = 16), ABL001 (n = 19), simvastatin (n = 17), and the combination of ABL001 and simvastatin (n = 19).

(C) Overall survival of mice injected intracardially with PC9 GR4-pFULT cells treated with DMSO (n = 9), ABL001 (n = 9), simvastatin (n = 9), and the combination (n = 9).

(D) Representative images (day 27 postinjection) of mice intracardially injected with PC9 BrM3-pFULT cells.

(E) Quantitative analysis (day 30 postinjection) of the whole body metastatic index in mice injected intracardially with PC9 BrM3 cells and treated with DMSO (n = 16), ABL001 (n = 19), simvastatin (n = 17), and the combination (n = 19). Data are the mean ± SEM.

(F) Immunofluorescence staining of brain tumors from PC9 BrM3 mice on day 35 stained with Ki67 (green), cleaved caspase 3 (c-C3) (red), and Hoescht 33342 (nuclei) (blue). Scale bars, 100 μm.

(G and H) Quantification of percent positive proliferative (G) and apoptotic (H) nuclei in tumor sections. Statistical analysis was performed using one-way ANOVA with Dunnett post hoc testing (n = 3). Data are the mean ± SEM. *$p < 0.05$. See Figure S6.

mitochondria for malignant transformation and growth (Vasan et al., 2020). Here we show that ABL allosteric inhibitors markedly decrease mitochondria function in lung cancer cells without affecting glycolysis. A CRISPR/Cas9 loss-of-function screen targeting metabolic enzymes revealed that HMGCR inactivation synergizes with ABL allosteric inhibitors at sublethal doses to induce metastatic lung cancer cell apoptosis, thereby revealing dual inactivation of the MVA pathway and ABL kinases as a strategy to augment apoptotic cell death and enhance therapeutic efficacy. Patients with lung cancer have the highest leading cancer-related mortality worldwide in part due to the lack of durable responses to current therapies resulting in metastatic and therapy-resistant disease progression (Herbst et al., 2018). By targeting unique metabolic vulnerabilities of metastatic lung cancer cells, we uncovered combination treatment strategies using available ABL allosteric inhibitors with FDA-approved statins for the treatment of therapy-resistant and brain-metastatic lung cancer cells in preclinical mouse models.

Dysregulation of the MVA pathway has been implicated in the progression of solid tumors, including glioblastoma, breast, and liver cancer (Clendening et al., 2010; Moon et al., 2019; Villa et al., 2016; Wang et al., 2017). Cancer cells exploit distinct bioactive end products generated by the MVA pathway, including cholesterol and isoprenoid intermediates, to promote tumor progression and therapy resistance. For example, glioblastomas rely on exogenous cholesterol for survival and

cholesterol depletion induces glioblastoma cell death (Villa et al., 2016). In contrast, we found that the synergistic interaction between ABL allosteric inhibitors and statins appears to be mediated by inhibition of protein prenylation and is independent of decreased cholesterol. Specifically, metabolic rescue of the geranylgeranylation pathway, but not cholesterol, was capable of rescuing cell survival in lung cancer cells cotreated with ABL001 and statins to an extent equivalent to MVA. Protein geranylgeranylation is required for processes such as protein and vesicular trafficking and cell proliferation (Wang and Casey, 2016). Multiple geranylgeranylated proteins might be targeted by statins in ABL-depleted cells. A recent report showed that lipophilic statins prevent membrane association of Rab11b, a small GTPase that regulates endosomal recycling and decreases breast cancer brain metastasis in mice (Howe et al., 2020). Among numerous substrates of the geranylgeranylation pathway are RAS-related GTPases, including members of the RAS and RHO-RAC families (Wang and Casey, 2016). Future studies are needed to assess whether decreased protein geranylgeranylation of specific targets mediates the decrease in lung cancer cell survival *in vitro* and in mouse models of metastasis following combination therapy with ABL001 and statins.

Previous reports have identified the potential of statins to function as anticancer agents; however, clinical trials using various chemotherapies in combination with statins have had either marginal or no effect on distant metastasis-free survival or overall survival in lung cancer patients with advanced disease (Han et al., 2011; Lee et al., 2017; Seckl et al., 2017). Retrospective analyses of various lung cancer patient cohorts have reported mixed findings regarding the impact of statin therapeutics on cancer-related mortality for patients taking statins at the onset of chemotherapy treatment (Cardwell et al., 2015; Khurana et al., 2007; Kuoppala et al., 2008; Wang et al., 2013). Our findings are consistent with clinical reports showing that statins added to first-line, standard-of-care chemotherapy do not impact the growth of primary lung adenocarcinoma tumors (Lee et al., 2017; Seckl et al., 2017) and suggest the potential use of ABL allosteric inhibitors in combination with statins for the treatment of advanced metastatic disease.

Whereas inactivation of ABL kinases impairs breast and lung cancer metastasis in mouse models (Gu et al., 2016, 2020; Hoj et al., 2019; Wang et al., 2016), clinical trials to treat breast and lung cancer patients with ABL ATP-site inhibitors have been ineffective in part due to targeting of multiple kinases other than ABL, possibly leading to paradoxical activation of cell survival pathways (Bauman et al., 2012; Chew et al., 2008; Cristofanilli et al., 2008; Dy et al., 2005; Johnson et al., 2003). Moreover, upon inhibiting the ABL kinases, the ATP-competitive inhibitors cause the ABL kinase SH3-SH2 cassette to remain in an open conformation while the allosteric inhibitors induce a closed conformation (Skora et al., 2013). In the open conformation, the SH3-SH2 domains can bind to downstream targets, but these domains are not accessible upon binding to ABL allosteric inhibitors. Notably, our recent work revealed that ABL allosteric inhibitors, but not ABL ATP-competitive inhibitors, disrupt the interaction between ABL2 and the HSF1 transcription factor (Hoj et al., 2020). This finding suggests that some protein-protein interactions dependent on distinct ABL protein conformations might be specifically disrupted by the binding of allosteric inhibitors to a unique site in the ABL kinase domain. Consistent with these findings, our work shows that the ABL allosteric inhibitors, which bind to the myristoyl-binding pocket in the C-lobe of the ABL kinase domain and are highly selective inhibitors of the ABL kinases, are capable of impairing mitochondria function in a manner similar to genetic inhibition of the ABL kinases, whereas the ATP-competitive inhibitors fail to impair mitochondrial function (Zhang et al., 2010). Thus, our findings support the potential use of ABL allosteric site inhibitors in combination with statins as a treatment strategy for lung cancer patients with advanced metastatic disease, including those patients with difficult-to-treat brain metastases or EGFR TKI resistance.

STAR★METHODS

Detailed methods are provided in the online version of this paper and include the following:

- KEY RESOURCES TABLE
- RESOURCE AVAILABILITY
  - Lead contact
  - Materials availability
  - Data and code availability
- EXPERIMENTAL MODEL AND SUBJECT DETAILS
  - Animal models
  - Cell lines and cell culture
- METHOD DETAILS
  - Pharmacologic inhibitor treatment studies
  - Seahorse measurements
  - MitoSOX staining
  - MitoTracker staining
  - Pooled CRISPR screen
  - Screen analysis
  - Cell viability assay
  - Colony formation assays
  - Annexin V staining
  - Immunoblotting procedures
  - Real-time quantitative PCR
  - Intracardiac injections
  - Subcutaneous flank xenografts
  - Orthotopic lung injection
  - Immunofluorescence and confocal microscopy
  - DNA plasmids
- QUANTIFICATION AND STATISTICAL ANALYSIS

SUPPLEMENTAL INFORMATION

Supplemental information can be found online at https://doi.org/10.1016/j.celrep.2021.109880.

ACKNOWLEDGMENTS

We thank Dr. Joan Massagué (Memorial Sloan Kettering Cancer Center, New York, NY) for providing the PC9 parental cells, Dr. Passi Jänne (Dana-Farber Cancer Institute, Boston, MA) for PC9-GR4 (gefitinib-resistant) cells (Cortot et al., 2013), and Dr. Fernando Lecanda (University of Navarra, Pamplona, Spain) for large-cell carcinoma (LCC) H460 cells. We thank the Duke University genome sequencing facility for providing assistance with deep sequencing data acquisition, the Duke Flow Cytometry Shared Resource for assistance

with fluorescence-activated cell sorting (FACS) analysis, the Duke Light Microscopy Core Facility, and the Duke Cancer Institute Bioinformatics Shared Resource. We are grateful to Dr. Donald McDonnell, Dr. Christopher Newgard, and Benjamin Mayro for critical reading of the manuscript and scientific advice. This work was supported by grants from the NIH (R01CA195549 and R01CA246133 to A.M.P., F31CA22496001 and F99CA245732-01 to J.P.H., R01CA207083 to K.C.W., F30CA206348 to K.H.L., and R01DK106090 to A.G.N. and N.J.M.), a Lung Cancer Research Foundation Free to Breathe Metastasis Research Grant (to A.M.P.), the Emerson Collective (A.M.P.), a Duke SPORE in Brain Cancer grant (P50CA190991 to A.M.P.), a National Science Foundation (NSF) Graduate Research Fellowship (DGE 1644868 to J.H.L.), the Duke Medical Scientist Training Program (T32GM007171 to K.H.L.), and a National Cancer Institute Cancer Center Support Grant (NCI CCSG award number P30CA014236 to Duke Cancer Institute). The content is solely the responsibility of the authors and does not necessarily represent the official views of the NIH.

AUTHOR CONTRIBUTIONS

Conceptualization, J.H.L., J.P.H., and A.M.P.; methodology, J.H.L., J.P.H., K.H.L., N.J.M., K.C.W., and A.M.P.; validation, J.H.L.; formal analysis, J.H.L., J.P.H., J.L., J.J.G., and A.M.P.; investigation, J.H.L., J.P.H., J.J.G., C.R., and A.G.N.; writing – original draft, J.H.L. and A.M.P.; writing – review & editing, J.H.L., J.P.H., K.H.L., J.L., N.J.M., K.C.W., and A.M.P.; visualization, J.H.L., J.P.H., J.J.G., and A.M.P.; supervision, A.M.P.; funding acquisition, A.M.P.

DECLARATION OF INTERESTS

A.M.P. is a consultant and advisory board member for The Pew Charitable Trusts. A.M.P. holds patent number U.S. 9,931,342 B2 related to this work. All other authors declare no competing interests.

Received: December 17, 2020
Revised: August 29, 2021
Accepted: October 4, 2021
Published: October 26, 2021

REFERENCES

Barter, P.J. (2018). High- versus low-dose statin: effects on cardiovascular events and all-cause death. Circulation *137*, 2013–2015.

Bauman, J.E., Eaton, K.D., Wallace, S.G., Carr, L.L., Lee, S.J., Jones, D.V., Arias-Pulido, H., Cerilli, L.A., and Martins, R.G. (2012). A phase II study of pulse dose imatinib mesylate and weekly paclitaxel in patients aged 70 and over with advanced non-small cell lung cancer. BMC Cancer *12*, 449.

Björkhem-Bergman, L., Lindh, J.D., and Bergman, P. (2011). What is a relevant statin concentration in cell experiments claiming pleiotropic effects? Br. J. Clin. Pharmacol. *72*, 164–165.

Cardwell, C.R., Mc Menamin, Ú., Hughes, C.M., and Murray, L.J. (2015). Statin use and survival from lung cancer: a population-based cohort study. Cancer Epidemiol. Biomarkers Prev. *24*, 833–841.

Chew, H.K., Barlow, W.E., Albain, K., Lew, D., Gown, A., Hayes, D.F., Gralow, J., Hortobagyi, G.N., and Livingston, R. (2008). A phase II study of imatinib mesylate and capecitabine in metastatic breast cancer: Southwest Oncology Group Study 0338. Clin. Breast Cancer *8*, 511–515.

Chou, C.W., Lin, C.H., Hsiao, T.H., Lo, C.C., Hsieh, C.Y., Huang, C.C., and Sher, Y.P. (2019). Therapeutic effects of statins against lung adenocarcinoma via p53 mutant-mediated apoptosis. Sci. Rep. *9*, 20403.

Clendening, J.W., Pandyra, A., Boutros, P.C., El Ghamrasni, S., Khosravi, F., Trentin, G.A., Martirosyan, A., Hakem, A., Hakem, R., Jurisica, I., and Penn, L.Z. (2010). Dysregulation of the mevalonate pathway promotes transformation. Proc. Natl. Acad. Sci. USA *107*, 15051–15056.

Cortot, A.B., Repellin, C.E., Shimamura, T., Capelletti, M., Zejnullahu, K., Ercan, D., Christensen, J.G., Wong, K.K., Gray, N.S., and Jänne, P.A. (2013). Resistance to irreversible EGF receptor tyrosine kinase inhibitors through a multistep mechanism involving the IGF1R pathway. Cancer Res. *73*, 834–843.

Cristofanilli, M., Morandi, P., Krishnamurthy, S., Reuben, J.M., Lee, B.N., Francis, D., Booser, D.J., Green, M.C., Arun, B.K., Pusztai, L., et al. (2008). Imatinib mesylate (Gleevec) in advanced breast cancer-expressing C-Kit or PDGFR-beta: clinical activity and biological correlations. Ann. Oncol. *19*, 1713–1719.

DeBerardinis, R.J., and Chandel, N.S. (2016). Fundamentals of cancer metabolism. Sci. Adv. *2*, e1600200.

Demidenko, E., and Miller, T.W. (2019). Statistical determination of synergy based on Bliss definition of drugs independence. PLoS ONE *14*, e0224137.

Deng, X., Okram, B., Ding, Q., Zhang, J., Choi, Y., Adrián, F.J., Wojciechowski, A., Zhang, G., Che, J., Bursulaya, B., et al. (2010). Expanding the diversity of allosteric bcr-abl inhibitors. J. Med. Chem. *53*, 6934–6946.

Dong, Y., Tu, R., Liu, H., and Qing, G. (2020). Regulation of cancer cell metabolism: oncogenic MYC in the driver's seat. Signal Transduct. Target. Ther. *5*, 124.

Dy, G.K., Miller, A.A., Mandrekar, S.J., Aubry, M.C., Langdon, R.M., Jr., Morton, R.F., Schild, S.E., Jett, J.R., and Adjei, A.A. (2005). A phase II trial of imatinib (ST1571) in patients with c-kit expressing relapsed small-cell lung cancer: a CALGB and NCCTG study. Ann. Oncol. *16*, 1811–1816.

Garrido, C., Galluzzi, L., Brunet, M., Puig, P.E., Didelot, C., and Kroemer, G. (2006). Mechanisms of cytochrome c release from mitochondria. Cell Death Differ. *13*, 1423–1433.

Gentleman, R.C., Carey, V.J., Bates, D.M., Bolstad, B., Dettling, M., Dudoit, S., Ellis, B., Gautier, L., Ge, Y., Gentry, J., et al. (2004). Bioconductor: open software development for computational biology and bioinformatics. Genome Biol. *5*, R80.

Gil-Henn, H., Patsialou, A., Wang, Y., Warren, M.S., Condeelis, J.S., and Koleske, A.J. (2013). Arg/Abl2 promotes invasion and attenuates proliferation of breast cancer in vivo. Oncogene *32*, 2622–2630.

Greuber, E.K., Smith-Pearson, P., Wang, J., and Pendergast, A.M. (2013). Role of ABL family kinases in cancer: from leukaemia to solid tumours. Nat. Rev. Cancer *13*, 559–571.

Gu, J.J., Hoj, J., Rouse, C., and Pendergast, A.M. (2020). Mesenchymal stem cells promote metastasis through activation of an ABL-MMP9 signaling axis in lung cancer cells. PLoS ONE *15*, e0241423.

Gu, J.J., Rouse, C., Xu, X., Wang, J., Onaitis, M.W., and Pendergast, A.M. (2016). Inactivation of ABL kinases suppresses non-small cell lung cancer metastasis. JCI Insight *1*, e89647.

Han, J.Y., Lee, S.H., Yoo, N.J., Hyung, L.S., Moon, Y.J., Yun, T., Kim, H.T., and Lee, J.S. (2011). A randomized phase II study of gefitinib plus simvastatin versus gefitinib alone in previously treated patients with advanced non-small cell lung cancer. Clin. Cancer Res. *17*, 1553–1560.

Hart, T., Chandrashekhar, M., Aregger, M., Steinhart, Z., Brown, K.R., Macleod, G., Mis, M., Zimmermann, M., Fradet-Turcotte, A., Sun, S., et al. (2015). High-resolution CRISPR screens reveal fitness genes and genotype specific cancer liabilities. Cell *163*, 1515–1526.

Herbst, R.S., Morgensztern, D., and Boshoff, C. (2018). The biology and management of non-small cell lung cancer. Nature *553*, 446–454.

Hoj, J.P., Mayro, B., and Pendergast, A.M. (2019). A TAZ-AXL-ABL2 feed-forward signaling axis promotes lung adenocarcinoma brain metastasis. Cell Rep. *29*, 3421–3434.e8.

Hoj, J.P., Mayro, B., and Pendergast, A.M. (2020). The ABL2 kinase regulates an HSF1-dependent transcriptional program required for lung adenocarcinoma brain metastasis. Proc. Natl. Acad. Sci. USA *117*, 33486–33495.

Howe, E.N., Burnette, M.D., Justice, M.E., Schnepp, P.M., Hedrick, V., Clancy, J.W., Guldner, I.H., Lamere, A.T., Li, J., Aryal, U.K., et al. (2020). Rab11b-mediated integrin recycling promotes brain metastatic adaptation and outgrowth. Nat. Commun. *11*, 3017.

Hu, M., Cheung, B.M., and Tomlinson, B. (2012). Safety of statins: an update. Ther. Adv. Drug Saf. *3*, 133–144.

Hughes, T.P., Mauro, M.J., Cortes, J.E., Minami, H., Rea, D., DeAngelo, D.J., Breccia, M., Goh, Y.T., Talpaz, M., Hochhaus, A., et al. (2019). Asciminib in chronic myeloid leukemia after ABL kinase inhibitor failure. N. Engl. J. Med. *381*, 2315–2326.

Jin, N., Bi, A., Lan, X., Xu, J., Wang, X., Liu, Y., Wang, T., Tang, S., Zeng, H., Chen, Z., et al. (2019). Identification of metabolic vulnerabilities of receptor tyrosine kinases-driven cancer. Nat. Commun. *10*, 2701.

Johnson, B.E., Fischer, T., Fischer, B., Dunlop, D., Rischin, D., Silberman, S., Kowalski, M.O., Sayles, D., Dimitrijevic, S., Fletcher, C., et al. (2003). Phase II study of imatinib in patients with small cell lung cancer. Clin. Cancer Res. *9*, 5880–5887.

Karr, S. (2017). Epidemiology and management of hyperlipidemia. Am. J. Manag. Care *23* (*9, Suppl*), S139–S148.

Kelly, W.J., Shah, N.J., and Subramaniam, D.S. (2018). Management of brain metastases in epidermal growth factor receptor mutant non-small-cell lung cancer. Front. Oncol. *8*, 208.

Khatri, A., Gu, J.J., McKernan, C.M., Xu, X., and Pendergast, A.M. (2019). ABL kinase inhibition sensitizes primary lung adenocarcinomas to chemotherapy by promoting tumor cell differentiation. Oncotarget *10*, 1874–1886.

Khurana, V., Bejjanki, H.R., Caldito, G., and Owens, M.W. (2007). Statins reduce the risk of lung cancer in humans: a large case-control study of US veterans. Chest *131*, 1282–1288.

Kienast, Y., von Baumgarten, L., Fuhrmann, M., Klinkert, W.E., Goldbrunner, R., Herms, J., and Winkler, F. (2010). Real-time imaging reveals the single steps of brain metastasis formation. Nat. Med. *16*, 116–122.

Konstantinopoulos, P.A., and Papavassiliou, A.G. (2007). Multilevel modulation of the mevalonate and protein-prenylation circuitries as a novel strategy for anticancer therapy. Trends Pharmacol. Sci. *28*, 6–13.

Kuoppala, J., Lamminpää, A., and Pukkala, E. (2008). Statins and cancer: a systematic review and meta-analysis. Eur. J. Cancer *44*, 2122–2132.

Kurmi, K., Hitosugi, S., Yu, J., Boakye-Agyeman, F., Wiese, E.K., Larson, T.R., Dai, Q., Machida, Y.J., Lou, Z., Wang, L., et al. (2018). Tyrosine phosphorylation of mitochondrial creatine kinase 1 enhances a druggable tumor energy shuttle pathway. Cell Metab. *28*, 833–847.e8.

Lee, Y., Lee, K.H., Lee, G.K., Lee, S.H., Lim, K.Y., Joo, J., Go, Y.J., Lee, J.S., and Han, J.Y. (2017). Randomized phase II study of afatinib plus simvastatin versus afatinib alone in previously treated patients with advanced nonadenocarcinomatous non-small cell lung cancer. Cancer Res. Treat. *49*, 1001–1011.

Lin, J., Gresham, J., Wang, T., Kim, S.Y., Alvarez, J., Damrauer, J.S., Floyd, S., Granek, J., Allen, A., Chan, C., et al. (2018). bcSeq: an R package for fast sequence mapping in high-throughput shRNA and CRISPR screens. Bioinformatics *34*, 3581–3583.

Lin, K.H., Xie, A., Rutter, J.C., Ahn, Y.R., Lloyd-Cowden, J.M., Nichols, A.G., Soderquist, R.S., Koves, T.R., Muoio, D.M., MacIver, N.J., et al. (2019). Systematic dissection of the metabolic-apoptotic interface in AML reveals heme biosynthesis to be a regulator of drug sensitivity. Cell Metab. *29*, 1217–1231.e7.

Lobell, R.B., Liu, D., Buser, C.A., Davide, J.P., DePuy, E., Hamilton, K., Koblan, K.S., Lee, Y., Mosser, S., Motzel, S.L., et al. (2002). Preclinical and clinical pharmacodynamic assessment of L-778,123, a dual inhibitor of farnesyl:protein transferase and geranylgeranyl:protein transferase type-I. Mol. Cancer Ther. *1*, 747–758.

Meirson, T., Genna, A., Lukic, N., Makhnii, T., Alter, J., Sharma, V.P., Wang, Y., Samson, A.O., Condeelis, J.S., and Gil-Henn, H. (2018). Targeting invadopodia-mediated breast cancer metastasis by using ABL kinase inhibitors. Oncotarget *9*, 22158–22183.

Merck (2020). Zocor (simvastatin) [package insert] (Merck).

Moon, S.H., Huang, C.H., Houlihan, S.L., Regunath, K., Freed-Pastor, W.A., Morris, J.P., 4th, Tschaharganeh, D.F., Kastenhuber, E.R., Barsotti, A.M., Culp-Hill, R., et al. (2019). p53 represses the mevalonate pathway to mediate tumor suppression. Cell *176*, 564–580.e19.

Munoz, M.A., Jurczyluk, J., Mehr, S., Chai, R.C., Arts, R.J.W., Sheu, A., McMahon, C., Center, J.R., Singh-Grewal, D., Chaitow, J., et al. (2017). Defective protein prenylation is a diagnostic biomarker of mevalonate kinase deficiency. J. Allergy Clin. Immunol. *140*, 873–875.e6.

Otahal, A., Aydemir, D., Tomasich, E., and Minichsdorfer, C. (2020). Delineation of cell death mechanisms induced by synergistic effects of statins and erlotinib in non-small cell lung cancer cell (NSCLC) lines. Sci. Rep. *10*, 959.

Packer, L.M., Rana, S., Hayward, R., O'Hare, T., Eide, C.A., Rebocho, A., Heidorn, S., Zabriskie, M.S., Niculescu-Duvaz, I., Druker, B.J., et al. (2011). Nilotinib and MEK inhibitors induce synthetic lethality through paradoxical activation of RAF in drug-resistant chronic myeloid leukemia. Cancer Cell *20*, 715–727.

Pavlova, N.N., and Thompson, C.B. (2016). The emerging hallmarks of cancer metabolism. Cell Metab. *23*, 27–47.

Perillo, B., Di Donato, M., Pezone, A., Di Zazzo, E., Giovannelli, P., Galasso, G., Castoria, G., and Migliaccio, A. (2020). ROS in cancer therapy: the bright side of the moon. Exp. Mol. Med. *52*, 192–203.

Plattner, R., Kadlec, L., DeMali, K.A., Kazlauskas, A., and Pendergast, A.M. (1999). c-Abl is activated by growth factors and Src family kinases and has a role in the cellular response to PDGF. Genes Dev. *13*, 2400–2411.

Pupo, E., Avanzato, D., Middonti, E., Bussolino, F., and Lanzetti, L. (2019). KRAS-driven metabolic rewiring reveals novel actionable targets in cancer. Front. Oncol. *9*, 848.

Reck, M., and Rabe, K.F. (2017). Precision diagnosis and treatment for advanced non-small-cell lung cancer. N. Engl. J. Med. *377*, 849–861.

Schneider, C.A., Rasband, W.S., and Eliceiri, K.W. (2012). **NIH Image to ImageJ: 25 years of image analysis.** Nat Methods *7*, 671–675.

Seckl, M.J., Ottensmeier, C.H., Cullen, M., Schmid, P., Ngai, Y., Muthukumar, D., Thompson, J., Harden, S., Middleton, G., Fife, K.M., et al. (2017). Multicenter, phase III, randomized, double-blind, placebo-controlled trial of pravastatin added to first-line standard chemotherapy in small-cell lung cancer (LUNGSTAR). J. Clin. Oncol. *35*, 1506–1514.

Shalem, O., Sanjana, N.E., Hartenian, E., Shi, X., Scott, D.A., Mikkelson, T., Heckl, D., Ebert, B.L., Root, D.E., Doench, J.G., and Zhang, F. (2014). Genome-scale CRISPR-Cas9 knockout screening in human cells. Science *343*, 84–87.

Skora, L., Mestan, J., Fabbro, D., Jahnke, W., and Grzesiek, S. (2013). NMR reveals the allosteric opening and closing of Abelson tyrosine kinase by ATP-site and myristoyl pocket inhibitors. Proc. Natl. Acad. Sci. USA *110*, E4437–E4445.

Tarrado-Castellarnau, M., de Atauri, P., and Cascante, M. (2016). Oncogenic regulation of tumor metabolic reprogramming. Oncotarget *7*, 62726–62753.

Thurnher, M., Nussbaumer, O., and Gruenbacher, G. (2012). Novel aspects of mevalonate pathway inhibitors as antitumor agents. Clin. Cancer Res. *18*, 3524–3531.

Valiente, M., Ahluwalia, M.S., Boire, A., Brastianos, P.K., Goldberg, S.B., Lee, E.Q., Le Rhun, E., Preusser, M., Winkler, F., and Soffietti, R. (2018). The evolving landscape of brain metastasis. Trends Cancer *4*, 176–196.

Valiente, M., Obenauf, A.C., Jin, X., Chen, Q., Zhang, X.H., Lee, D.J., Chaft, J.E., Kris, M.G., Huse, J.T., Brogi, E., and Massagué, J. (2014). Serpins promote cancer cell survival and vascular co-option in brain metastasis. Cell *156*, 1002–1016.

Vasan, K., Werner, M., and Chandel, N.S. (2020). Mitochondrial metabolism as a target for cancer therapy. Cell Metab. *32*, 341–352.

Vicent, S., Luis-Ravelo, D., Antón, I., García-Tuñón, I., Borrás-Cuesta, F., Dotor, J., De Las Rivas, J., and Lecanda, F. (2008). A novel lung cancer signature mediates metastatic bone colonization by a dual mechanism. Cancer Res. *68*, 2275–2285.

Villa, G.R., Hulce, J.J., Zanca, C., Bi, J., Ikegami, S., Cahill, G.L., Gu, Y., Lum, K.M., Masui, K., Yang, H., et al. (2016). An LXR-cholesterol axis creates a metabolic co-dependency for brain cancers. Cancer Cell *30*, 683–693.

Wang, J., Li, C., Tao, H., Cheng, Y., Han, L., Li, X., and Hu, Y. (2013). Statin use and risk of lung cancer: a meta-analysis of observational studies and randomized controlled trials. PLoS ONE *8*, e77950.

Wang, J., and Pendergast, A.M. (2015). The emerging role of ABL kinases in solid tumors. Trends Cancer *1*, 110–123.

Wang, J., Rouse, C., Jasper, J.S., and Pendergast, A.M. (2016). ABL kinases promote breast cancer osteolytic metastasis by modulating tumor-bone interactions through TAZ and STAT5 signaling. Sci. Signal. *9*, ra12.

Wang, M., and Casey, P.J. (2016). Protein prenylation: unique fats make their mark on biology. Nat. Rev. Mol. Cell Biol. *17*, 110–122.

Wang, X., Huang, Z., Wu, Q., Prager, B.C., Mack, S.C., Yang, K., Kim, L.J.Y., Gimple, R.C., Shi, Y., Lai, S., et al. (2017). MYC-regulated mevalonate metabolism maintains brain tumor-initiating cells. Cancer Res. *77*, 4947–4960.

Warren, C.F.A., Wong-Brown, M.W., and Bowden, N.A. (2019). BCL-2 family isoforms in apoptosis and cancer. Cell Death Dis. *10*, 177.

Wood, W.G., Eckert, G.P., Igbavboa, U., and Müller, W.E. (2010). Statins and neuroprotection: a prescription to move the field forward. Ann. N Y Acad. Sci. *1199*, 69–76.

Wylie, A.A., Schoepfer, J., Jahnke, W., Cowan-Jacob, S.W., Loo, A., Furet, P., Marzinzik, A.L., Pelle, X., Donovan, J., Zhu, W., et al. (2017). The allosteric inhibitor ABL001 enables dual targeting of BCR-ABL1. Nature *543*, 733–737.

Xie, Y. (2016). Dynamic Documents with R and knitr, Second Edition (CRC Press).

Yang, H., Liang, S.Q., Schmid, R.A., and Peng, R.W. (2019). New horizons in *KRAS*-mutant lung cancer: dawn after darkness. Front. Oncol. *9*, 953.

Zhang, J., Adrián, F.J., Jahnke, W., Cowan-Jacob, S.W., Li, A.G., Iacob, R.E., Sim, T., Powers, J., Dierks, C., Sun, F., et al. (2010). Targeting Bcr-Abl by combining allosteric with ATP-binding-site inhibitors. Nature *463*, 501–506.

Zong, W.X., Rabinowitz, J.D., and White, E. (2016). Mitochondria and cancer. Mol. Cell *61*, 667–676.

Zorov, D.B., Juhaszova, M., and Sollott, S.J. (2014). Mitochondrial reactive oxygen species (ROS) and ROS-induced ROS release. Physiol. Rev. *94*, 909–950.

STAR★METHODS

KEY RESOURCES TABLE

REAGENT or RESOURCE	SOURCE	IDENTIFIER
Antibodies		
Cleaved PARP	Cell Signaling	Cat# 5625; RRID: AB_10699459
Total PARP	Cell Signaling	Cat# 9532; RRID: AB_659884
Cleaved Caspase-3	Cell Signaling	Cat # 9661; RRID: AB_2341188
Caspase-3	Cell Signaling	Cat# 9668; RRID:AB_2069870
Phospho-CrkL (Tyr207)	Cell Signaling	Cat# 3181; RRID:AB_331068
Cytochrome C	Cell Signaling	Cat# 11940; RRID:AB_2637071
beta-Catenin	Cell Signaling	Cat# 8480; RRID:AB_11127855
beta-Tubulin (D2N5G)	Cell Signaling	Cat# 15115; RRID:AB_2798712
Ki67	Cell Signaling	Cat# 9449; RRID:AB_2797703
CRKL (C-20)	Santa Cruz	Cat# sc-319; RRID:AB_631320
GAPDH (6C5)	Santa Cruz	Cat# sc-32233; RRID:AB_627679
RAP1	Santa Cruz	Cat# sc-398755; RRID:AB_2884025
HMGCR	Millipore	Cat# ABS229; RRID:AB_11203328
HDJ2	Thermo Fisher	Cat# MA5-12748; RRID:AB_10982482
TdTomato	Kerafest	Cat# EST203; RRID:AB_2732803
Goat anti-Mouse IgG (H+L) Cross-Adsorbed Secondary Antibody, Alexa Fluor 488	Thermo Fisher	Cat# A-11001; RRID:AB_2534069
Goat anti-Rabbit IgG (H+L) Highly Cross-Adsorbed Secondary Antibody, Alexa Fluor 633	Thermo Fisher	Cat# A-21070; RRID:AB_2535731
Goat anti-Rat IgG (H+L) Cross-Adsorbed Secondary Antibody, Alexa Fluor 568	Thermo Fisher	Cat# A-11077; RRID:AB_141874
Peroxidase AffiniPure Goat Anti-Mouse IgG (H+L)	Jackson Immunoresearch	Cat# 115-035-003; RRID:AB_10015289
Peroxidase AffiniPure Goat Anti-Rabbit IgG (H+L)	Jackson Immunoresearch	Cat#115-035-144; RRID: AB_2307391
Chemicals, Peptides, and Recombinant Proteins		
GNF-5 (Abl kinase small molecule inhibitor)	Duke Small Molecule Synthesis Facility	N/A
ABL001 (Asciminib)	Duke Small Molecule Synthesis Facility	N/A
Simvastatin	Cayman	Cat# 10010344; CAS: 79902-63-9
Gefitinib	Sigma-Aldrich	Cat# SML1657; CAS: 184475-35-2
Fluvastatin	Sigma-Aldrich	Cat# SML0038; CAS: 93957-55-2
Mevalonolactone	Sigma-Aldrich	Cat# M4667; CAS: 674-26-0
Cholesterol	Sigma-Aldrich	Cat# C3045; CAS: 57-88-5
Geranylgeranyl pyrophosphate	Sigma-Aldrich	Cat# G6025; CAS: 6699-20-3
Farnesyl pyrophosphate	Sigma-Aldrich	Cat# F6892; CAS: 13058-04-3
FTI-277	Tocris	Cat# 2407; CAS: 1217447-06-7
GGTI-298	Tocris	Cat# 2430; CAS: 1217457-86-7
Docetaxel	LC Laboratories	Cat# D-1000; CAS: 114977-28-5
Rotenone	Sigma-Aldrich	Cat# R8875; CAS: 83-79-4
Antimycin A	Sigma-Aldrich	Cat# A8674; CAS: 1397-94-0
Oligomycin	Sigma-Aldrich	Cat# 75351; CAS: 579-13-5

(*Continued on next page*)

Continued

REAGENT or RESOURCE	SOURCE	IDENTIFIER
Critical Commercial Assays		
Seahorse XF96 V3 PS Cell Culture Microplates	Agilent	Cat# 101085-004
Seahorse XF Cell Mito Stress Test Kit	Agilent	Cat# 103015-100
MitoSOX Red Mitochondrial Superoxide Indication	Thermo Fisher	Cat# M36008
MitoTracker Red CMXRos	Thermo Fisher	Cat# M7512
Cell Titer Glo	Promega	Cat# G7571
PE Annexin V Apoptosis Detection Kit I	BD Biosciences	Cat# 559925
Cell Fractionation Kit	Cell Signaling	Cat# 9038
Hoescht 33342 Solution	Thermo Fisher	Cat# 62249
Deposited Data		
PC9 cells transduced with LOF CRISPR/Cas9 metabolism library treated with vehicle or GNF5 sequencing files	This paper	BioProject: PRJNA679091
Experimental Models: Cell Lines		
PC9	Valiente et al. (2014)	N/A
PC9 GR4	Cortot et al. (2013)	N/A
PC9 BrM3	Hoj et al. (2019)	N/A
H460	Vicent et al. (2008)	N/A
H358	ATCC	Cat# CRL-5807, RRID:CVCL_1559
Experimental Models: Organisms/Strains		
Mouse outbred athymic nu/nu	Jackson Laboratory	007850; RRID:IMSR_JAX:007850
Oligonucleotides		
See Table S3 for a list of all primers and oligonucleotides		
Recombinant DNA & Plasmids		
pLKO-puro Non-Target shRNA Control	Sigma Mission TRC1	SHC016-1EA
pLKO-puro shHMGCR 46448	Sigma Mission TRC1	TRCN00000046448
pLKO-puro shHMGCR 46452	Sigma Mission TRC1	TRCN00000046452
Scramble control shRNA	Gu et al. (2016)	N/A
ABL1 shRNA	Gu et al. (2016)	N/A
ABL2 shRNA	Gu et al. (2016)	N/A
Software and Algorithms		
PC9 cells transduced with LOF CRISPR/Cas9 metabolism library treated with vehicle or GNF5 code repository	This paper	https://doi.org/10.5281/zenodo.5530434
Prism 6 and 8	Graphpad	https://graphpad.com/scientific-software/prism
ImageJ	(Schneider et al., 2012)	https://imagej.nih.gov
RStudio	R Foundation for Statistical Computing	https://rstudio.com
Living Image	Perkin Elmer	https://perkinelmer.com
Knitr	Foundation for Open Access Statistics	https://yihui.org/knitr/
bcSeq	Bioconductor	https://bioconductor.org/packages/release/bioc/html/bcSeq.html

RESOURCE AVAILABILITY

Lead contact

Further information and requests for resources and reagents should be directed to, and will be fulfilled by, the corresponding author and Lead Contact, Ann Marie Pendergast (ann.pendergast@duke.edu).

Materials availability

All unique and stable reagents generated in this study are available from the Lead Contact upon completion of a Materials Transfer Agreement.

Data and code availability

- CRISPR dataset has been deposited at BioProject and is publicly available as of the date of publication. Accession number is listed in the key resources table.
- All original code has been deposited at Zenodo and is publicly available as of the date of publication. DOI is listed in the key resources table.
- Any additional information required to reanalyze the data reported in this paper is available from the lead contact upon request.

EXPERIMENTAL MODEL AND SUBJECT DETAILS

Animal models

All procedures involving mice were approved and performed following the guidelines of the IACUC of Duke University Division of Laboratory Animal Resources. All studies employed 8-12-week old age-matched female outbred athymic nu/nu mice (#007850; RRID: IMSR_JAX:007850) purchased from The Jackson Laboratory. The mice were maintained under pathogen-free conditions in the Duke Cancer Center Isolation Facility for immune-deficient mice.

Cell lines and cell culture

PC9 parental cells were a gift from Dr. Joan Massagué (Memorial Sloan Kettering Cancer Center, New York, NY, USA) (Valiente et al., 2014). PC9-GR4 (gefitinib-resistant) cells were a gift from Dr. Passi Jänne (Dana-Farber Cancer Institute, Boston, MA, USA) (Cortot et al., 2013). Large cell carcinoma (LCC) H460 cells were provided by Dr. Fernando Lecanda (University of Navarra, Pamplona, Spain) (Vicent et al., 2008). PC9-BrM3 cell lines were derived in the Pendergast laboratory by serial intracardiac injection as previously described (Hoj et al., 2019). Human H358 lung cancer cells were purchased from ATCC. Parental and derivative cell line pairs were subjected to short tandem repeat (STR) profiling through the Duke University DNA Analysis Facility Human cell line authentication (CLA) service to confirm their authenticity. Lung cancer cells were maintained in RPMI 1640 (Life Technologies) supplemented with 10% tetracycline-screened fetal bovine serum (FBS, Hyclone), 10 mM HEPES, 1 mM sodium pyruvate, and 0.2% glucose. H293T cells used for transfection and virus production were purchased from ATCC and were maintained in DMEM (Life Technologies) with 10% FBS (Corning). All cultures were maintained at 37°C in humidified air containing 5% CO_2.

METHOD DETAILS

Pharmacologic inhibitor treatment studies

For experiments assessing effects of pharmacologic inhibitors *in vitro* (GNF-5, ABL001, Gefitinib, Docetaxel, Simvastatin, Fluvastatin, FTI-277, GGTI-298), drugs were dissolved in DMSO and the final concentration of DMSO in culture media did not exceed 0.1% v/v. Cholesterol was solubilized in 40% (2-hydroxypropyl)- β-cyclodextrin at room temperature, sterile filtered (0.45 μM) and stored at −20°C. MVA was resolved with 0.1M NaOH, followed by neutralizing with 0.1M HCL/1M HEPES. The ABL allosteric inhibitors GNF-5 and ABL001 were synthesized by the Duke University Small Molecule Synthesis Facility and validated by LC-MS and 1H-NMR, as well as cell-based assays. The following drugs used for *in vitro* analysis were purchased from: Cayman: Simvastatin (10010344); Sigma: Gefitinib (SML1657), Fluvastatin (SML0038), Mevalonolactone (M4667), Cholesterol (C3045), Geranylgeranyl pyrophosphate (G6025), Farnesyl pyrophosphate (F6892); Tocris: FTI-277 (2407) and GGTI-298 (2430); LC Laboratories: Docetaxel (D-1000).

Seahorse measurements

Basal and maximal oxygen consumption rate and ATP production were measured using a Mito Stress test Kit and a Glycolytic Rate Kit was used to measure basal and compensatory glycolysis. Both kits used a XF96 Extracellular Flux Analyzer (Seahorse Bioscience) to measure changes according to manufacturer's instructions. Cells were plated in XF96 plates at 10,000 cells per well on Day 0. Cells were treated on Day 1 with IC_{50} doses of GNF5, ABL001, gefitinib, docetaxel, and vehicle control. For rescue experiments, cells were treated with 2.5 μM ABL001, 1 μM simvastatin, 500 μM MVA, 5 μM GGTI-298, 12.5 μM FTI-277. On the day of the Seahorse run, media was aspirated and replaced with XF Assay Medium (Seahorse Bioscience) supplemented with 10 mM glucose, 1 mM

pyruvate, and 2 mM glutamine supplemented with corresponding drug or vehicle. The plate was incubated in a non-CO2 incubator at 37°C for 1hr to equilibrate. OCR measurements, taken every 6min, were collected at baseline and after the sequential addition of oligomycin 1 μM (final concentration), FCCP 0.5 μM, and rotenone 0.75 μM + antimycin A 1.5 μM. Data were normalized to total nuclei count per well.

MitoSOX staining

MitoSOX was purchased from Thermofisher (cat. M36008). 100,000 cells were plated in six-well plates and treated with vehicle or IC_{50} doses of indicated drugs for 24hr. Cells were stained with 5 μM MitoSOX resuspended in serum-free RPMI containing associated drug concentration in the dark for 10 mins in a 37°C 5% CO2 incubator. Cells were washed once with PBS and trypsinized followed by another wash in PBS and resuspended in 500 μL of PBS. The samples were analyzed using flow cytometer BD FACSCanto II. Gating strategy was defined using untreated/unstained cells. Analysis of flow cytometry data was performed with FlowJo v10.

MitoTracker staining

MitoTracker Red CMXRos was purchased from Thermofisher (cat. M7512). 100,000 cells were plated in six-well plates and treated with vehicle or IC_{50} doses of GNF5. Cells were stained with 100 nM MitoTracker resuspended in serum-free RPMI containing associated drug concentration in the dark for 30 mins in a 37°C 5% CO2 incubator. Cells were washed once with PBS and trypsinized followed by another wash in PBS and resuspended in 500 μL of PBS. The samples were analyzed using flow cytometer BD FACS Canto II. Gating strategy was defined using untreated/unstained cells. Analysis of flow cytometry data was performed with FlowJo v10.

Pooled CRISPR screen

PC9 cells were seeded into 12 six-well plates at 0.25e6 cells/well. A separate plate was also prepared for no puromycin and puromycin controls of non-transduced cells. Cells were transduced at a MOI of 0.2. 24 hours after viral transduction, cells were replated into puromycin-containing media. A sample was collected after 48 hours of puromycin exposure to confirm library coverage in the transduced population. Transduced cells were expanded in puromycin for a total of 10 days prior to drug introduction, at which point the transduced cell population was split into vehicle (DMSO) and GNF5 treatment conditions and maintained for up to two weeks. Cells were treated with 2 μM GNF5 which corresponded to 20%–30% loss in cell viability following a 3-day dose-response assay. Cells were counted and replated every 2 days with drug being replenished every day. At any given point during the screen, each replicate was represented by a minimum of 12E6 cells, sufficient to provide 1000x coverage of the library (~1000 cells per unique sgRNA). Samples of 25E6 cells were collected upon screen initiation, termination, and at weekly intervals. Following completion of the screens, DNA was extracted (DNeasy Blood & Tissue Kit, QIAGEN) and prepared for sequencing as previously described (Shalem et al., 2014).

Screen analysis

Deep sequencing was performed on an Illumina Nextseq platform (75 bp, paired-ended) to identify differences in library composition. All sequencing was performed by the Duke University genome sequencing facility. Barcoded reads were mapped to the guide RNA library using bcSeq (Lin et al., 2018) to obtain the counts for each guide RNA. Determinations of genetic essentiality and drug sensitization/resistance were made by evaluating differential guide compositions between the initial population and subsequent drug-treated and vehicle-treated cell populations. Briefly, the fractional representation (FR) for the guide reads within a sample was normalized to the total reads attributed to that sample. A direct comparison between two samples was represented by the quotient of the respective FRs in the log2 scale, which we term the depletion metric (DM). The guide-level DMs for each gene were then collapsed to gene-level scores by taking the average of the top three most depleted constructs resulting in a biased analysis focused on depleted genes. Genes represented by fewer than 5 guides per condition were excluded from analysis. In the 2,322-gene library, 7 genes (representing 0.3% of the total library) were excluded. Genetic essentiality was calculated by considering the depletion/enrichment of the vehicle-treated (DSMO) population over time (DMSO final / DSMO initial). Drug sensitization/resistance was calculated by considering the depletion/enrichment of the drug-treated population relative to the vehicle-treated population (Drug final / DMSO final). All depletion/enrichment effects are reported as log2 ratios. All analyses were conducted using the R statistical environment (https://www.r-project.org/) along with extension packages from the comprehensive R archive network (CRAN; https://cran.r-project.org/) and the Bioconductor project (Gentleman et al., 2004). The analyses were carried out with adherence to the principles of reproducible analysis using the knitr package (Xie, 2016) for generation of dynamic reports and gitlab for source code management. The code for replicating the statistical analysis was made accessible through a public source code repository: https://doi.org/10.5281/zenodo.5530434. Because many metabolic genes are known to be essential to cellular viability (Hart et al., 2015), determining the effect of cell-essential genetic loss on apoptosis is difficult. To this point, a subset of essential metabolic genes will have lost representation in our screen before the 10-day puromycin selection period is over; our screen does not capture the effect of these genes (which represent a trivial fraction of our library) on apoptosis.

The remaining cell-essential genes are captured by the screen. Since our analysis normalizes the effect of gene knockout + drug treatment to gene knockout alone, the interpretation of these genes does not require additional correction, except that they necessarily suffer from reduced resolution.

Cell viability assay

Cells were seeded in white-walled clear bottom 96-well plates in triplicate at 3,000 cells per well. Each condition was run in triplicate wells each from three independent experiments and measured using CellTiter-Glo reagent (Promega). Plates were read on a Tecan Infinite M1000 Microplate Reader and results were analyzed in GraphPad.

Colony formation assays

Cells were seeded in 12-well plates in duplicate at 1,000 cells per well for PC9 and PC9 GR4 cell lines and at 250 cells per well for H460 cells (n = 2). Cells were treated with 1 μM ABL001, 100 nM Simvastatin, or combination of ABL001 and Simvastatin for 1 week. Cells were then fixed with methanol and stained with crystal violet. Images were taken using an Epson scanner. 1 mL of 10% acetic acid was added per well and a plate reader was used to measure absorbance at 590 nm.

Annexin V staining

Annexin V staining was performed to determine the percentage of cells undergoing apoptosis. 100,000 cells were plated in six-well plates and treated with vehicle, 10 μM GNF5, 1 μM Simvastatin, 0.5 μM Fluvastatin or the combination for 24hr. Upon collection, cells were trypsinized, washed twice with PBS, resuspended in 100 μL 1X Annexin V binding buffer (BD Biosciences) containing 5 μL Annexin V stain conjugated to APC (allophycocyanin) (BD Biosciences). Phosphatidylserine externalization was measured using APC-conjugated Annexin. Following a 15min incubation at RT, the samples were analyzed using flow cytometer BD FACSCanto II. Gating strategy was defined using untreated/unstained cells. Analysis of flow cytometry data was performed with FlowJo v10.

Immunoblotting procedures

Cells were lysed in RIPA buffer (50 mM Tris-HCl pH 7.4, 150 mM NaCl, 1 mM EDTA, 1% Triton X-100, 1% sodium deoxycholate and 0.1% SDS) containing protease-phosphatase inhibitor cocktail (Cell Signaling). Cell suspensions were rotated at 4C for 15 minutes followed by microcentrifugation to remove cell debris, and protein concentration was quantified using the DC Protein Assay (BioRad). Equal amounts of protein were separated by SDS/PAGE and transferred onto nitrocellulose membranes using the Trans-blot Turbo Transfer system (Bio-Rad). Membranes were incubated with primary antibody overnight at 4oC, followed by 3 washes in 1xTBST and incubation with corresponding secondary antibody for 1 h at room temperature. Blots were developed using SuperSignal West PLUS Chemiluminescent Substrate developing solution (Invitrogen) and imaged using either film or a ChemiDoc XRS+ imager (Bio-Rad). The following antibodies used for immunoblot analysis were purchased from: Cell Signaling: Phospho-CrkL (Tyr207) (3181L), beta-Tubulin (D2N5G) (15115S), cleaved PARP (5625), total PARP (9542), cleaved caspase 3 (9661), total caspase 3 (9668), cytochrome C (11940), beta-Catenin (8480); Thermofisher: HDJ2 (MA5-12748); Millipore Sigma: ABL1 (8E9) (MAB1130), ABL2 (6D5) (H00000027-M03); Santa Cruz: RAP1 (sc-398755), CRKL (C-20) (sc-319), GAPDH (6C5) (sc-32233); Jackson Immunoresearch: Peroxidase AffiniPure Goat Anti-Mouse IgG (H+L) (115-035-003), Peroxidase AffiniPure Goat Anti-Rabbit IgG (H+L) (115-035-144).

Real-time quantitative PCR

RNA was isolated from subconfluent monolayers of cancer cells using the RNeasy RNA isolation kit (QIAGEN), and cDNA synthesis was performed using oligo(dT) primers and M-MLV reverse transcriptase (Invitrogen). RT-qPCR was performed in triplicate wells using iTaq Universal SYBR Green Supermix (Bio-Rad). Primers used in this study were purchased from Sigma Aldrich. Analysis of real-time data was collected using a Bio-Rad CFX384 machine and CFX Maestro software. Expression levels of each gene were normalized to GAPDH control housekeeping genes using the ddCT algorithm. Primers sequences used: BBC3 Fwd (GACCTCAACGCA CAGTACGAG), BBC3 Rev (AGGAGTCCCATGATGAGATTGT), Bcl2 Fwd (GGTGGGGTCATGTGTGTGG), Bcl2 Rev (CGGTTCAGG TACTCAGTCATCC), Bcl2L1 Fwd (GAGCTGGTGGTTGACTTTCTC), Bcl2L1 Rev (TCCATCTCCGATTCAGTCCCT).

Intracardiac injections

All animal experiments were conducted in accordance with protocols approved by the Duke University Division of Laboratory Animal Resources Institutional Animal Care and Use Committee (IACUC). Cells were stably transduced with pFU-luciferase-Tomato (pFuLT) DNA prior to injection to allow for bioluminescent imaging (BLI) *in vivo*. We used 8-12-week old age-matched female athymic nu/nu mice for all studies (Jackson Laboratory). Mice were anesthetized with 5% isoflurane prior to injections. For all studies, $4x10^5$ lung cancer cells suspended in 100 μL PBS were injected into the left cardiac ventricle with a 30-gauge needle. Animals were monitored until full recovery from anesthesia and were subsequently imaged weekly to both confirm proper anatomical injection and to monitor for progression of disease burden using an IVIS XR bioluminescent imager. The ABL allosteric inhibitor ABL001 (Asciminib) was used for *in vivo* inhibition of the ABL kinases in tumor-bearing mice and was prepared as a suspension in sterile 0.5% methylcellulose/0.5% Tween-80 as described previously (Wylie et

al., 2017). Mice were treated with either vehicle control or 100 mg/kg/qd ABL001 via oral gavage once per day. ABL001 was synthesized by the Duke University Small Molecule Synthesis Facility and validated by LC-MS and 1H-NMR. Simvastatin was purchased from Toronto Research Chemicals (cat. S485000) and dissolved in aqueous 2% dimethyl sulfoxide (DMSO), 30% polyethylene glycol 400 (PEG 400), and 5% Tween 80. Mice were treated with either vehicle control or 10 mg/kg/qd simvastatin. To account for potential interactions between the two drugs and solvents, mice were treated each morning with either simvastatin or vehicle control, and two hours later with either ABL001 or vehicle control via oral gavage. The presence of brain metastases was confirmed through *in vivo* BLI followed by isolation of brains for OCT or paraffin sectioning. Living Image software was used for analysis of BLI data.

Subcutaneous flank xenografts

Mice were injected subcutaneously with 1e6 PC9 GR4 cells re-suspended in growth factor reduced Matrigel matrix in the back right flank. Mice were stratified into treatment groups once the tumors reached an average of 50 mm^3. The animals were drug treated for a total of 3 weeks and tumor volume was measured weekly by a caliper. At the end of the study, mice were euthanized, and tumors were extracted for image collection.

Orthotopic lung injection

PC9 pFuLT lung cancer cells were used for orthotopic lung injection into athymic nude mice. Mice were anesthetized with 4% isoflurane and placed in the left lateral decubitus position. PC9 pFuLT cells were re-suspended in PBS solution, and 50 μL of the cell suspension was injected percutaneously into the right lateral thorax at the lateral dorsal axillary line. The needle was quickly inserted approximately 6 mm into the thorax and quickly removed. Mice were turned to the right lateral decubitus position following tumor cell injection. Respiratory rate was monitored throughout the entire procedure, and mice were observed for 30 min until fully recovered. Body weights and wound healing was monitored weekly. Injected mice were treated with either vehicle (0.5% methylcellulose, 0.5% Tween-80), ABL001, Simvastatin, or combination of ABL001 and Simvastatin starting on day 6 post-injection for 36 days. Mice were monitored weekly for tumor growth via bioluminescent imaging (BLI) using the IVIS XR imaging system.

Immunofluorescence and confocal microscopy

Brains were perfused and fixed with 4% paraformaldehyde in PBS prior to extraction. Upon extraction, brains were rotated overnight (O/N) in 4% paraformaldehyde in PBS at 4°C followed by subsequent washes in PBS the following day. For OCT embedding, brains underwent sucrose protection in 15% sucrose in water at 4°C O/N rotation following by O/N rotation in 30% sucrose in water at 4°C before OCT embedding at −80°C. OCT sections were 10 μm thick. For paraffin embedding, brains were placed into 70% ethanol prior to paraffin embedding. Paraffin embedding was performed at the Duke University Immunohistopathology Core Facility sections were cut at 5 μm thick. OCT sections were thawed at room temperature for 15 minutes followed by acetone fixation. Paraffin sections were deparaffinized, rehydrated, and heat inactivated (BioCare Medical Decloaking Chamber). Both deparaffinized and OCT sections were then washed in PBS and blocked in 3% goat serum in PBS with 0.05% Tween-20 for one hour. Sections were incubated with primary antibodies in blocking solution overnight at 4°C in a humidified chamber at concentrations indicated below. Sections were then washed with PBS followed by incubation with the appropriate secondary antibody in blocking solution for one hour at room temperature. Sections were then washed with PBS, incubated with the nuclear stain, Hoechst33342, and washed again with PBS before mounting using aqueous mounting media (Dako-S3025). Antibodies for immunofluorescence and IHC experiments included: cleaved caspase 3 (Cell Signaling 9661) at 1:100 dilution, Ki67 (Cell Signaling 9449) at 1:200 dilution, tdTomato (Kerafast EST203) at 1:100 dilution. All images were captured on an Axio Imager D10 (Carl Zeiss) with a 20 × /0.75 EC Plan-Neofluar objective lens. Mitochondrial morphology analysis was performed by plating 75,000 H460 cells on glass coverslips in 12-well plates. Cells were treated with IC_{50} doses of each drug the following day. After 24 hours, the cells were stained with 100 nM MitoTracker Red CMXRos (Thermofisher cat. M7512) for 30 min, fixed (formaldehyde), permeabilized (Triton-X), stained with Hoescht 33342 and mounted. The slides were imaged using a Zeiss 880 inverted confocal Airyscan microscope with 63x oil objective. For all representative images in the manuscript, experiments were conducted at least twice, and had no repeatability issues. Mitochondrial morphology was determined using the tubeness and vesselness algorithms in Fiji. Mitochondrial fragmentation versus connectivity was determined by plotting length × width of several thousand mitochondrial from at least 10 cells across at least two independent experiments.

DNA plasmids

Sequences for shRNAs targeting the ABL kinases were as follows: scrambled shRNA (GGTGTATGGGCTACTATAGAA); ABL1 shRNA (GGTGTATGAGCTGCTAGAGAA); ABL2 shRNA (CCTTATCTCACCCACTCTGAA). Stable non-inducible shRNAs against non-target control (NTC) and HMGCR in the pLKO.1 vector were from the Sigma Mission TRC1 Lentiviral shRNA library and were obtained through the Duke Functional Genomics Shared Resource Facility. Sequences and Sigma clone identifiers for each of these shRNAs were as follows: HMGCR shRNA 46448 (CCGGGCAGTGATAAAGGAGGCATTTCTCGAGAAATGCCTCCTTTATCACTGCTTTTTG) and HMGCR shRNA 46452 (CCGGCCTGCTGCTATAAATTGGATACTCGAGTATCCAATTTATAGCAGCAGGTTTTTG).

QUANTIFICATION AND STATISTICAL ANALYSIS

Statistical analyses were performed using GraphPad Prism 7 and GraphPad Prism 9 software. Mouse numbers per group were determined through statistical power calculations where 10 mice per group allows for 90% power, at the unadjusted 0.05 two-sided level, to detect inter-group differences of 50% and assuming intra-group differences of 25%. For Kaplan-Meier survival curves, p values were calculated using log-rank (Mantel-Cox) testing. P values below an adjusted $p < 0.017$ were deemed significant accounting for 3 pairwise comparisons. Statistical analysis of tumor flux was evaluated by ANOVA followed by Fisher post hoc testing to calculate p values and those less than 0.05 were quantified as statistically significant. For comparisons between mouse groups of unequal size, the mean value and SEM were used to allow for statistical analysis by ANOVA. Bar graph data represent averages ± SEM.